Proceedings of the International Conference

Numerical Methods for Scientific Computations and Advanced Applications

(NMSCAA'16)

In cooperation with

siam

Editor

Krassimir Georgiev

May 29 – June 2, 2016, Hissar, Bulgaria

Sofia 2016

IICT

Institute of Information and Communication Technologies
Bulgarian Academy of Sciences

Proceedings of the International Conference

Numerical Methods for Scientific Computations and Advanced Applications (NMSCAA'16)

May 29 – June 02, 2016, Hissarya, Bulgaria

Krassimir Georgiev (Editor)

Institute of Information and Communication Technologies
Bulgarian Academy of Sciences

In cooperation with

siam

Sofia, 2016

Numerical Methods for Scientific Computations and Advanced Applications
(NMSCAA'16)

Proceedings of the International Conference

Printed in Sofia, Bulgaria

PREFACE

This book contains papers presented during the International Conference on "Numerical Methods for Scientific Computations and Advanced Applications" (NMSCAA'16), May 29–June 2, 2016, Hissarya, Bulgaria. The conference was organized by the Institute of Information and Communication Technologies, Bulgarian Academy of Sciences in cooperation with Society for Industrial and Applied Mathematics (SIAM).

The Conference Specific topics of interest are as follows: (a) Multiscale and multiphysics problems; (b)Robust preconditioning; (c) Monte Carlo methods; (d) Optimization and control systems; (e) Scalable parallel algorithms; (f) Advanced computing for innovations.
The list of the plenary invited speakers includes: Owe Axelsson (Institute of Geonics, ASCR, Czech Republic); Raytcho Lazarov (TA&MU, College Station, USA); Zahari Zlatev (Aarhus University, Denmark) and Clemens Hofreither (Johannes Kepler University, Linz, Austria).
The Scientific Computing is one of the most prominent examples of a interdisciplinary area involving mathematics, computer science, engineering, physics, chemistry, medicine etc. The tools of Scientific Computing are usually based on mathematical models and corresponding computer codes that are used to perform virtual experiments to obtain new data or to better understand existing experimental results. Numerical Analysis is one of the crucial elements of Scientific Computing. It develops and analyzes numerical methods for discretization of continuous models and their subsequent solution, as well as for approximation of discrete data, such as: data interpolation and extrapolation, methods for solving linear and non-linear systems of algebraic equations (direct and iterative solution methods, preconditioning, multilevel and multigrid methods, etc.), methods for solving systems of ordinary and partial differential equations, methods for solving integral equations, and optimization problems.
Next to Numerical methods and the scientific computations are the Advanced Applications – the implementation of the developed numerical methods into computer codes and their customization for the numerous computing systems and for solving a number of real life problems.

Krassimir Georgiev

May 2016

Contents

Part A

Extended abstracts[1]

[1] Arranged alphabetically according to the family name of the first author.

Analysis of Numerical Approximations to Degenerate Differential Equations

Ivanka Tr. Angelova, Lubin G. Vulkov

1 Introduction

The interest of differential equations with boundary degeneration is motivated by their numerous applications. As a simple, but typical for our purpose, is the one-factor short-term rate model of finance described by the stochastic differential equation

$$dS_t = (a + bS)dt + \sigma S^{\alpha} dW_t, \tag{1}$$

where $W(t)$, $t \geq 0$ is a standard Brownian motion, a, b and σ are positive constants, and $\alpha \geq 0$ is a specified number as most often being 0, 0.5 or 1, see e.g [8]. The corresponding to (1) PDE satisfied by the price $V(S,t)$ takes the form

$$\frac{\partial V}{\partial t} + \frac{1}{2}\sigma^2 S^{2\alpha}\frac{\partial^2 V}{\partial S^2} + (a + bS)\frac{\partial V}{\partial S} - rV = f(S,V),\ 0 < S < \infty,\ t > 0. \tag{2}$$

It is often solved with terminal condition $V(S,T) = V_T(S)$. The main difficulties at numerical solution of the problem are the *degeneration* of equation (2) at $S = 0$ and the *semi-infinite interval* $(0,\infty)$. In this talk we concentrate only on the *degeneration*. Let use note that applying suitable transformation to (2), it can be transformed to another one solved on the interval $(0,1)$ but in the new PDE appears another degeneration at the right end, see e.g. [3]. For nonlinear models see [5,6].
We discretize the Black-Sholes operator (2) in time introducing functions
$V_j(S) \approx V(S,t_j)$, $t_j = j\triangle t$, $j = 0,1,\ldots,J$ and truncate $(0,\infty)$ to $(0,S_{max})$:

$$\frac{1}{2}\sigma^2 S^{2\alpha} V_j'' + (a + bS)V_j' - \left(r - \frac{1}{\triangle t}\right)V_j = \frac{1}{\triangle t}V_{j-1} + f(S,V_j),\ V_0(S) = V_T(S). \tag{3}$$

Further we discuss the behavior of V^j and its derivatives at $S \to 0$ on two ODE boundary value problems (BVP). The first one is as follows:

$$-(x^{2\alpha}p(x)u')' + q(x)u = f(x),\ ' \equiv d/dx,\ x \in (0,1),\ \ u(1) = 0. \tag{4}$$

The authors of [2] prescribe appropriate (weighted) homogeneous boundary condition at the origin and prove existence and uniqueness of $H^2_{loc}(0,1]$ solutions. The case $0 < \alpha < 0.5$ is important for us and it is proved that:
$\lim_{x\to 0} u(x) = 0$, $u \in C^{0,1-\alpha}[0,1]$, $\|u\|_{C^{0,1-\alpha}} \leq C\|f\|_{L_2}$, $x^{\alpha}u' \in H^1(0,1)$, $\|x^{\alpha}u'\|_{H^1} \leq C\|f\|_{L_2}$. The constant C only depend on α. Also, there exists a function $f \in C_0^{\infty}(0,1)$ such that near the origin

$$u(x) = a_1 x^{1-2\alpha} + a_2 x^{3-4\alpha} + a_3 x^{5-6\alpha} + \cdots,\ a_1 \neq 0,\ \text{therefore } u' \sim x^{-2\alpha}.$$

Next, given $0.5 \le \alpha < 0.75$ and $f \in L^2(0,1)$, there exists $u \in H^2_{loc}(0,1)$ satisfying (4) with the properties $\lim_{x\to 0}(1-\ln x)^{-0.5}u(x) = 0,\ \lim_{x\to 0+} x^{2\alpha-1}u'(x) = 0$.
Further, given $\alpha \ge 1$ and $f \in L^2(0,1)$, there exists solution of (4) $u \in H^2_{loc}(0,1)$ with the properties: $\lim_{x\to 0+} x^{0,5\alpha}u(x) = 0,\ \lim_{x\to 0+} x^{1.5\alpha}u'(x) = 0$.
Next, we consider the following BVP with a small parameter ε (whose reduced equation, $\varepsilon = 0$, is our subject, so called elliptic *regularization*):

$$L[u] \equiv -(\varepsilon+x)^{\beta}u'' - a(x)u' + b(x)u = f(S.V),\ 0 < x < 1,\ u(0) = A_0,\ u(1) = A_1, \quad (5)$$

where $0 < \varepsilon \le 1,\ \beta = 1$ or $\beta = 2$ and $a(x),\ b(x) \in C[0,1]$, $c(x) \ge m_0 > 0$. The following estimates are established in [7]. Let $u(x,\varepsilon)$ be the solution to (5) with $\beta = 1$. Then if $a = a(0) > 0$ we have

$$|u^{(k)}(x,\varepsilon)| \le M \begin{cases} (x+\varepsilon)^{1-a-k} & 0 < a < 1, \\ 1 + (\varepsilon+x)^{-k}\ln^{-1}\varepsilon^{-1} & a = 1, \\ 1 + \varepsilon^{a-1}(\varepsilon+x)^{1-a-k} & a > 1. \end{cases} \quad (6)$$

Let $u(x,\varepsilon)$ be the solution of (5) with $\beta = 2$ and $a = a(0) > 0$. Then for $k \le m$

$$|u^{(k)}(x,\varepsilon)| \le M[1 + \varepsilon^{-2k}\exp(-\alpha a x/\varepsilon^2)],\ 0 < \alpha < 1,\ 0 < x < 1. \quad (7)$$

The purpose of this study is to develop effective numerical methods based on *elliptic regularization* for linear (European option) and semi-linear (American options) degenerate parabolic equations starting from ODEs of type (3).

2 Numerical analysis of Problem (4)

Using the above estimates for behavior of the solution and its derivatives we construct adequate approximations. Let consider on $[0,1]$ system of mesh points: $0 = x_0 < ... < x_i < ... < x_N = 1$ such that $x_i = (ih)^{\mu},\ i = 0,\dots N,\ \mu \ge 1,\ hN = 1$. Let denote

$$I^{\alpha}[g;a,b] = \int_a^b \frac{g(x)}{x^{2\alpha}}dx.\ \xi = \xi(\alpha;a,b) = \frac{I^{\alpha}[x;a,b]}{I^{\alpha}[1;a,b]}.$$

The finite difference scheme is:

$$p(\xi_{i-1/2})\frac{U_i - U_{i-1}}{\hbar_i I^{\alpha}[1;x_{i-1},x_i]} + p(\xi_{i+1/2})\frac{U_i - U_{i+1}}{\hbar_i I^{\alpha}[1;x_i,x_{i+1}]} + q_i U_i = f_i, \quad (8)$$

$\hbar_i = \xi_{i+1/2} - \xi_{i-1/2},\ \xi_{i-1/2} = \xi(\alpha;x_{i-1},x_i),\ \xi_{i+1/2} = \xi(\alpha;x_i,x_{i+1}),\ i = 1,\dots,N-1$

Then in agrement of the above estimates, see also [2] for more details, $U_0 = 0$ for Dirichlet problem and

$$(2-2\alpha)p(\xi_{1/2})(U_0 - U_1)/h^2 + q(0)U_0 = f(0) - p(0)(2-2\alpha)/x_1$$

for Neumann problem at $0 \le \alpha < 0.5$, $p(0)(U_0 - U_1)/h^2 + q(0)U_0 = f(0)$, at $0.5 \le \alpha < 1$. We rewrite (8) in the form $-a_i U_{i-1} + c_i U_i - b_i U_{i+1} = f_i$ or $A_N U^N = f^N$ whit

$U^N = (U_1, \ldots, U_{N-1})^T$. It is well known that the numerical method for the original problem, construction of the mesh domain, basic functions, etc. are chosen such that the *condition number* $c(A_N) = \|A_N^{-1}\|\|A_N\|$ be as possible as small. We discuss $c(A_N)$ for our approximations and the effect of the preconditioning on Table 1. Multiplied A_N by $D = diag\{c_i^{-1}\}$ we get $B_N = DA_N$ and multiplied A_N by $D = diag\{\hbar_i/h\}$ we get $C_N = DA_N$, i.e. we do diagonal *preconditioning*.

Table 1: $Example1.$: $\alpha = 0.25$.

	$n=1,\ O(h^2)$			$n=2,\ O(h^4)$		
N	$c(A)/N^2$	$c(B)/N^2$	$c(C)/N^2$	$c(A)/N^6$	$c(B)/N^2$	$c(C)/N^4$
32	20.2645	0.3781	0.4633	0.0454	0.2468	0.0301
64	30.2193	0.3783	0.4761	0.0378	0.2467	0.0170
128	44.2661	0.3784	0.4842	0.0317	0.2467	0.0091
256	64.0575	0.3784	0.4893	0.0266	0.2467	0.0048
512	91.9496	0.3784	0.4925	0.0224	0.2467	0.0025
1024	131.2875	0.3784	0.4945	0.0181	0.2467	0.0012

The conclusion is that the preconditioning improves significantly the condition numbers. Different approach to problem (4) for $p(x) = \varepsilon$ is proposed in [4].

3 Numerical analysis of Problem (5)

On the base of the estimates (6) we propose the following numerical method for $\beta = 1$. Let introduce the graded mesh $0 = x_0 < ... < x_i < ... < x_N = 1$ such that $q_i = ih,\ i = 0, \ldots N,\ hN = 1$. $x_i = x(q_i) = (\varepsilon^{1-\beta} + pq))^{1/(1-\beta)} - \varepsilon,\ p = 1 + \varepsilon)^{1-\beta}) - \varepsilon^{1-\beta}$, $\beta = (a+2)/3$. Then consider the finite difference scheme:

$$-\frac{(\varepsilon + x_i)^\beta}{\hbar_i}\left(\frac{U_{i+1} - U_i}{h_{i+1}} - \frac{U_i - U_{i-1}}{h_i}\right) - a(x_i)\frac{U_{i+1} - U_i}{h_{i+1}} + c(x_i)U_i = f(x_i). \quad (9)$$

One can prove uniform with respect to ε convergence of the discrete solution U to the exact one u with rate of convergence $O(h),\ h = \max_i h_i$.
Now on the base of the estimates (7), we solve (5) at $\beta = 2$ on the Shishkin mesh: $e = 2(\varepsilon \ln N)^2;\ \tau = \min(1/2, e);\ h = 2\tau/N;\ H = 2(1-\tau)/N$, such that $x_i = ih,\ i = 0, \ldots N/2,\ x_i = \tau + (i-1)H,\ i = N/2+1, \ldots,\ N$ by the finite difference scheme (9). Again, one can prove the same convergence as in the case $\beta = 1$.
We prove that the condition numbers on graded meshes (Liseikin and Shishkin, respectively) depend on the small parameter ε. But the simple diagonal preconditioning improves the situation. The numerical experiments confirm this, see Table 2.
Acknowledgments: The research of the second author was supported by the European Union under Grand Agreement number 304617 (FP7 Marie Curie Action Project Multi-ITN STRIKE- Novel Methods in Computational Finance) and the Bulgarian National Fund of Science under Project I20/2014.

Table 2: $\varepsilon = 10^{-2}$.

	$\beta = 1$		$\beta = 2$	
N	$c(A)/N^2$	$c(B)/N^2$	$c(A)/N^2$	$c(B)/N^2$
32	4.7944	0.3611	143.1072	0.1239
64	6.5943	0.3633	101.5252	0.1126
128	9.1688	0.3644	84.7166	0.1080
256	12.8370	0.3649	80.2668	0.1061
512	18.0496	0.3652	83.5742	0.1054
1024	25.4434	0.3653	93.1358	0.1054

References

[1] I. Angelova , L. Vulkov. $O(h^2, h^4, ...)$ approximations of a singular Sturm-Liouvile equation. IN: AIP Conf. Proc, American Institute of Physics, (2012), 160-167.

[2] H. Castro, H. Wang. A singular Sturm-Liouville equation under homogeneous boundary conditions, J. of Funct. Anal., (2011), 1542-1590.

[3] T. Chernogorova, R. Valkov. Analysis of a FVEM fpr a degemerate parabolic equation in the zero-coupon bond pricing, Comp. Appl. Math., (2015), 619-646.

[4] C. Grosmann, L. Ludwig, H. Roos, Layer-adapted methods for a singularly perturved singular problem, Comp. Methods in Appl. Math., V. 11, (2011), 192-205.

[5] M.N.Koleva, Efficient numerical methods for solving Cauchy problem for Gamma equation, AIP, v. 1410 (2011), 120-127

[6] M.N. Koleva, Positivity preserving numerical method for non-linear Black-Sholes models, LNCS, v.8236 (2013), 363-370

[7] V. D. Liseikin, Layer Resolving Grids and Transformations for Singular Perturbation Problems, VVSP, 2011.

[8] K. Mikula, D. Sevcovic, B. Stehlikova, Analytical and Numerical Methods for Pricing Financial Derivatives, Nova Science Publishers Inc., Hauppauge, 2011.

On Improving the QRN Generation Performance on Intel MIC Architectures

Emanouil Atanassov, Mariya Durchova, Todor Gurov, Sofiya Ivanovska, and Aneta Karaivanova

The Monte Carlo methods are an important tool used for simulating and modeling complex processes. Due to the excellent parallelisation properties of Monte Carlo methods they are widely used as part of workloads run on modern supercomputers. However, the typical rate of convergence of Monte Carlo methods of $\frac{1}{\sqrt{N}}$ leads to the necessity to use large numbers of samples to achieve acceptable convergency [4]. The so-called quasi-Monte Carlo methods attempt to replace the pseudo-random numbers in Monte Carlo methods with specially crafted, deterministic sequences, whose distribution is more even [1]. The uniformity of distribution of these sequences is usually measured by their discrepancy and consequently, the sequences with convergence rate of their discrepancy of $\mathcal{O}(N^{-1}\log^s(N))$, where s is the dimension, are called "low-discrepancy sequences". This rate of convergence is conjectured to be the best possible. Many such sequences have been investigated both in theory and practice. Some of the most popular families of low-discrepancy sequences are those of Sobol and Halton [2, 3, 5].

The increasing complexity of the supercomputers creates new challenges to the efficient use of the available hardware resources. One of the most notable tendency today is the use of General Purpose GPU computing technologies, typically provided by NVIDIA GPUs, or Intel MIC architecture, implemented on Intel Xeon Phi accelerators. The systems that employ accelerators have much better energy efficiency, but reach huge counts of computing cores or threads that have to be managed and introduce additional levels where parallelisation and optimisation of algorithms has to be performed. In the NVIDIA GPGPUs there is the concept of threads that execute simultaneously, essentially running the same code on different data, loosely following the SIMD model.

The Intel Xeon Phi accelerators have internal organization that is more "traditional" in the sense that they offer certain number of cores and the possibility for 4× hyperthreading (one core may run up to 4 independent threads. However, if one tries to simply recompile his or her code for Xeon Phi, the performance of the resulting application will not be impressive, because the individual cores of a Xeon Phi accelerator are rather slow when considered as a generic CPU. Their real computing power can only be tapped if one uses their capability for vector processing. The Intel MIC architecture provides instructions that allow whole vectors of real numbers to be processed. It is precisely this capability of Xeon Phi accelerators that allows supercomputers built with them to achieve high results in the LINPACK benchmark with good energy efficiency. Although the Intel compilers can make use of vector instructions when processing user codes, the results are far from optimal in most cases. Monte Carlo methods have a certain logical organization that is not very amenable to

this type of automatic vectorization. Motivated by the starting of operations of the new Bulgarian supercomputer, deployed at the Institute of Information and Communication Technologies, which has 150 dual-socket nodes HP SL250s Gen8 with 2 Intel Xeon E5-CPU E5-2650 v2 @ 2.60GHz and 2 Intel Xeon Phi 7120P co-processors, we investigated various approaches for developing efficient quasi-Monte Carlo algorithms to run on this machine.

Typically the generation of a quasi-random number sequence takes substantial part of the whole execution time and has more complex structure than a usual pseudo-random number generator. It is well established in theory and practice of quasi-Monte Carlo methods that some way of introducing randomness to the sequences is beneficial. Some of these so-called "scrambling" schemes add substantial number of operations [6].

In our work we concentrated on the families of sequences of Sobol and Halton as they are perhaps the most used in quasi-Monte Carlo methods and the methods used for them can be extended to some other families that are close to them. For example, the Niederreiter sequences are very similar to the Sobol sequences and our methods and codes can easily be extended to them [3, 6]. For the Halton sequences it is well known that if they are used without modification and in algorithms with high constructive dimension, the results will be affected by a certain correlation between consecutive dimensions [2, 5]. Unless unrealistically high number of samples is achieved, these correlations will introduce bias.

The "scrambling" schemes avoid these problems, but the modification, introduced by Atanassov, offers a better theoretical basis, since the rate of convergence of the modified sequence has better theoretically guaranteed value than that for the unmodified sequence [2, 3]. Nevertheless our computer codes can deal with both cases as well as other potential scramblings.

Our experience was the direct use of the special vector instructions is not that difficult and achieves substantial improvement in performance. In the next listing one can see how the (modified) Halton sequence can be generated, using the Intel compiler intrinsics for the vector instructions.

```
 Is32vec16 r2= * (Is32vec16*)&sequence.lastdigit[i];
r2 = Is32vec16 ( _mm512_add_epi32 ( r2, _mm512_set1_epi32(1) ));
__mmask16 somemask;
Is32vec16 p1=* (Is32vec16*)&sequence.primes[i];
somemask= _mm512_cmpge_epi32_mask(r2,p1);
r2=Is32vec16 (_mm512_mask_sub_epi32(r2, somemask, r2,p1));
* (Is32vec16*)&sequence.lastdigit[i]=r2;
r2 = * (Is32vec16*)&sequence.perturbedlastdigit[i];
Is32vec16 modif= * (Is32vec16*)&sequence.modifiers[0][i];
r2 = Is32vec16(_mm512_add_epi32(r2,modif));
__mmask16 othermask= _mm512_cmpge_epi32_mask(r2,p1);
r2=Is32vec16 (_mm512_mask_sub_epi32(r2,othermask,r2,p1));
* (Is32vec16*)&sequence.perturbedlastdigit[i]=r2;
F64vec8 iparts = *(F64vec8 *)& sequence.partsums[1][i];
```

```
F64vec8 inveprimes = *(F64vec8 *)& sequence.inveprimes[i];;
F64vec8 pdigit = _mm512_cvtepi32lo_pd( r2);
F64vec8 oparts = _mm512_fmadd_pd ( pdigit, inveprimes ,iparts);
*(F64vec8*)&sequence.partsums[0][i]=oparts;
iparts = *(F64vec8 *)& sequence.partsums[1][i+8];
inveprimes= *(F64vec8 *)& sequence.inveprimes[i+8];
__m512i pmm=_mm512_extload_epi64(& ((__m256i *)&r2)[1],
_MM_UPCONV_EPI64_NONE ,_MM_BROADCAST_4X8 ,_MM_HINT_NONE );
pdigit = _mm512_cvtepi32lo_pd( pmm);
oparts = _mm512_fmadd_pd ( pdigit, inveprimes ,iparts);
*(F64vec8*)&sequence.partsums[0][i+8]=oparts;
if (somemask){
int dd=1;
for (int k=0;k<FLOATSINWORD;k++,dd+=dd){
if (somemask & dd ){
sequence.blastdigit[i+k]++;
if (sequence.blastdigit[i+k]==sequence.primes[i+k]){
sequence.blastdigit[i+k]=0;
}
```

This admittedly complicated code is in the innermost cycle of the generation routine. Operations that are done on all terms of the sequence are done in the first part of the code, while some masks are also formed that allow operations that are to affect only part of terms to be applied using these masks. Although the code becomes very difficult to read, its users do not need to understand the details.
Our comparizons of vectorized vs non-vectorized versions of this code show important improvement from using the vector instructions. For example, on one core of the Intel Xeon Phi 5110P accerator, available on our older servers, the non-vectorized version generates 10 million terms of the sequence with dimensionality 160 for $4m25s = 265s$, while the vector versions does that in $48s$ or approximately 5 times faster.
If all the cores of Intel Xeon Phi are used, the same computation is done by the vector version for $1.2s$, if 120 threads are used. Here we note that there are some peculiarities of the Intel MIC architecture, which make it a requirement to use hyper-threading if one wants to use the maximum performance of the vector units of Intel Xeon Phi. If only 60 threads are used instead of 120, the same computation requires 1.5s.
The main consideration when developing our vectorized generation routines has been to avoid logical statements and you can see in the above code snipped how the masks are used to this effect.

Acknowledgments

This work was supported by the National Science Fund of Bulgaria under Grant #DFNI-I02/8 and by the European Commission under H2020 project VI-SEEM (Contract Number 675121).

References

[1] E. Atanassov, A. Karaivanova, T. Gurov, S. Ivanovska, M. Durchova, D. Sl. Dimitrov, Quasi-Monte Carlo Integration on the Grid for Sensitivity Studies, Earth Science Informatics Journal, Vol. 3, Issue 4, pp. 289-296, 2010.

[2] E. I. Atanassov, On the discrepancy of the Halton sequences, Math. Balkanica, New Series 18.1âĂŞ2, pp. 15âĂŞ32, 2004.

[3] E. Atanassov, A New Efficient Algorithm for Generating the Scrambled Sobol Sequence, Numerical Methods and Applications, Springer, LNCS 2542, pp. 83-90, 2003.

[4] H. Chi and E. Jones, Generating Parallel Quasirandom Sequences by using Randomization, Journal of distributed and parallel computing, 67(7), pp. 876-881, 2007.

[5] J. H. Halton, On the efficiency of certain quasi-random sequences of points in evaluating multi-dimensional integrals, Numer. Math., 2, pp. 84-90, 1960.

[6] A.Owen, Scrambling Sobol and Niederreiter-Xing Points. Journal of Complexity, 14(4), pp. 466-489, 1998.

Arbitrarily Accurate Preconditioners by Low Rank Approximations of Inverse Schur Complement Matrices

Owe Axelsson

Many important problems involve an unfeasibly high degree of computational complexity unless properly handled to allow an acceptable computer time. Examples are optimal control problems constrained by partial differential equations (PDEs) and time dependent problems on a long time frame. In such problems one must solve the PDE s many times. Due to the large size of the problems, iterative solution methods must be used. Thereby it is crucial to construct preconditioner that leads to a small condition number that holds uniformly with respect to all problem parameters, including discretization mesh sizes.

In this work we consider symmetric and positive definite PDEs split in two-by-two block matrix from correspondingly to some splitting of the mesh nodes. The preconditioner involves inverses of the Schur complement matrices. We show that they can be arbitrarily accurately approximated by low rank correction terms to the inverses of block-diagonal matrices. The method involves computation of some eigenvectors to the Schur complement matrix, preconditioned by the inverses of the block-diagonal matrices. Computing a sufficient number of such eigenvectors, that can be done adaptively, enables reaching a uniformly bounded condition number, arbitrarily close to unity. Since the PDE problem must be solved many times, the initial cost to compute such eigenvectors can be small related to the total cost.

In this talk we first present the basic idea of the low rank corrections to the inverses of the Schur complement matrices, when using exact eigenvectors. Then it is shown that it suffices to compute vectors that span a subspace, sufficiently close to the subspace spanned by the exact eigenvectors. Methods to compute the approximate eigenvectors are given,

Finally, it is commented on various ways to split the mesh nodes to get a proper two-by-two block form of the matrix. The method is applicable for both coarse-fine mesh splitting and for domain decomposition splittings. The basic idea of the method is as follows.

Given $\mathcal{A} = \begin{bmatrix} A_I & A_{IC} \\ A_{CI} & A_C \end{bmatrix}$, an spd matrix, where A_I, A_C have orders $m \times m$ and $n \times n$, respectively, and $m > n$. In our applications, A_C is a coarse mesh matrix and $m \gg n$. Consider first a block-triangular matrix preconditioner on inverse matrix form,

$$\begin{bmatrix} A_I^{-1} & 0 \\ -\widetilde{S}^{-1}A_{CI}A_I^{-1} & \widetilde{S}^{-1} \end{bmatrix} \begin{bmatrix} A_I & A_{IC} \\ A_{CI} & A_C \end{bmatrix} = \begin{bmatrix} I & A_I^{-1}A_{IC} \\ 0 & \widetilde{S}^{-1}S \end{bmatrix} \tag{1}$$

where $S = A_C - A_{CI}A_I^{-1}A_{IC}$ is the Schur complement matrix and its inverse is approximated by $\widetilde{S}^{-1} = A_C^{-1} + \sigma_q V S_V^{-1} V^T$, $\sigma_q > 0$, $S_V = V^T S V$, $V = [\mathbf{v}_1, \mathbf{v}_2, \cdots, \mathbf{v}_q]$, $1 \leq q < m_0 = m - rank(A_{IC})$.

Let $\{\gamma_i^2, \mathbf{v}_i\}_{i=1}^n$ be the eigensolutions of the generalized eigenvalue problem

$$\gamma^2 A_C \mathbf{v} = A_{CI} A_I^{-1} A_{IC} \mathbf{v}, \tag{2}$$

$\mathbf{v}_i^T \mathbf{v}_j = \delta_{ij}$, i.e., the eigenvectors are orthogonal and normalized. Assume also that the eigenvalues are ordered in a decreasing order as $1 > \gamma_1^2 \geq \gamma_2^2 \cdots \geq \gamma_k^2$, where $\gamma_k = 0$ for $k = m_0, \cdots, n$.
It holds that $S\mathbf{v}_i = (1-\gamma_i^2) A_C \mathbf{v}_i$, so $S^{1/2}\mathbf{v}_i = (1-\gamma_i^2) S^{1/2} A_C S^{1/2} \mathbf{v}_i$. Further,

$$S^{1/2} \widetilde{S}^{-1} S^{1/2} = S^{1/2} A_C^{-1} S^{1/2} + \sigma_q S^{1/2} V S_V^{-1} V^T S^{1/2} = S^{1/2} A_C^{-1} S^{1/2} + \sigma_q P,$$

where $P = \widetilde{V}(\widetilde{V}^T \widetilde{V})^{-1} \widetilde{V}^T$, $\widetilde{V} = S^{1/2} V$ is a projection matrix,

$$P\widetilde{\mathbf{v}}_i = \begin{cases} \widetilde{\mathbf{v}}_i, & 1 \leq i \leq q \\ 0, & q+1 \leq i \leq n, \end{cases}$$

with $\widetilde{\mathbf{v}}_i = S^{1/2}\mathbf{v}_i$. It follows that the eigenvalues of $\widetilde{S}^{-1}S$ equal

$$\lambda_i(\widetilde{S}^{-1}S) = \begin{cases} 1 - \gamma_i^2 + \sigma_q, & 1 \leq i \leq q \\ 1 - \gamma_i^2, & q+1 \leq i \leq n. \end{cases}$$

To make the lower bounds equal, we let $\sigma_q = \gamma_i^2 - \gamma_{q+1}^2$. Then

$$1 - \gamma_{q+1}^2 \leq \lambda_i(\widetilde{S}^{-1}S) \leq \begin{cases} 1, & \text{if } \gamma_q^2 + \gamma_{q+1}^2 \geq \gamma_1^2, \\ 1 - \gamma_q^2 + \gamma_1^2 - \gamma_{q+1}^2, & \text{if } \gamma_q^2 + \gamma_{q+1}^2 < \gamma_1^2. \end{cases}$$

Hence, for the condition number of $\widetilde{S}^{-1}S$ it holds

$$\varkappa(\widetilde{S}^{-1}S) \leq \begin{cases} \frac{1}{1-\gamma_{q+1}^2}, & \text{if } \gamma_q^2 + \gamma_{q+1}^2 \geq \gamma_1^2, \\ 1 + \frac{\gamma_1^2 - \gamma_q^2}{1-\gamma_{q+1}^2}, & \text{if } \gamma_q^2 + \gamma_{q+1}^2 < \gamma_1^2. \end{cases}$$

It is seen that we have reduced the condition number from $\varkappa(A_C^{-1}S) = \frac{1}{1-\gamma_1^2}$ to $\max\{\frac{1}{1-\gamma_{q+1}^2}, 2\}$, by moving the smallest eigenvalues $1-\gamma_i^2$, $i = 1, 2, \cdots, q$ to the upper part of the spectrum, near the unit value.
The matrix S_V, of order $q \times q$, takes the form

$$S_V = V^T S V = \left[\mathbf{v}_i (1-\gamma_j^2) A_C \mathbf{v}_j\right]_{i,j=1}^q.$$

Its computation requires matrix-vector multiplications with A_C and q^2 inner products of vectors of order n. Hence, in practice, q cannot be very large and the correction is of low rank.
By use of an adaptive method we show also that we can in fact reduce the condition number to become arbitrarily close to unity and that the method can be applied to approximate the whole inverse of $\mathcal{A}$.

Reduced Order Modelling of a Coupled Chemotaxis–Haptotaxis Model for Cancer Invasion

Gabriel Dimitriu

There exists a vast literature concerning mathematical analysis of different reaction-diffusion-taxis that have been applied to describe the cancer invasion, angiogenesis, cancer chemotherapy treatments, etc. (see for example [2],[3] and references therein). In this work, we carry out an application of DEIM reduced order method (a Discrete version of "Empirical Interpolation Method", introduced by Barrault et al. in [1]) combined with Proper Orthogonal Decomposition (POD) to provide dimension reduction of a model introduced in [3]. This model describes a process of cancer cell invasion of tissue (extracellular matrix – ECM), taking into account the role of the generic matrix degrading enzyme such as urokinase-type plasminogen activator (uPA), chemotaxis and haptotaxis. This DEIM method applied to this model eliminates the major disadvantage of POD, where the nonlinear reduced terms still have to be evaluated on the original state space making the simulation of the reduced-order system too expensive.
The model governing the interactions between the tumour cells, extracellular matrix and uPA is defined by the following 2D system of reaction-diffusion-taxis equations:

$$\begin{aligned} c_t &= \underbrace{D_c\nabla^2 c}_{dispersion} - \underbrace{\nabla\cdot(\chi_c c\nabla u)}_{chemotaxis} - \underbrace{\nabla\cdot(\xi_c c\nabla v)}_{haptotaxis} + \underbrace{\mu_1 c(1-c-v)}_{proliferation}, \\ v_t &= \underbrace{-\delta u v}_{proteolysis} + \underbrace{\mu_2 v(1-c-v)}_{renewal}, \\ u_t &= \underbrace{D_u\nabla^2 u}_{Diffusion} + \underbrace{\alpha c}_{production} - \underbrace{\beta u}_{decay}. \end{aligned} \tag{1}$$

The state variables in (1) have the following significance: $c(x,y,t)$ represents the density of cancer cells, $v(x,y,t)$ is the density of extracellular matrix macromolecules, and $u(x,y,t)$ is the concentration of uPA protease. The positive constants D_c and D_u are the diffusion coeficients, the positive parameters χ_c and ξ_c represent the chemotactic and haptotactic sensitivities, and μ_1, μ_2, α, β, δ are positive rate constants.
In order to close the system (1) boundary and initial conditions for c, u and v are required. According to an *in vitro* experimental protocol in which invasion takes place within an isolated system, one assumes that there is no-flux of tumour cells or uPA protease accross the boundary of the domain. The initial conditions are mathematically defined by negative exponential functions, initially assuming that there is a cluster of cancer cells already present, and that they penetrated a short distance into the extracellular matrix, while the remaining space is accupied by the matrix alone. For the uPA protease initial concentration, we assume that it is proportional to the initial tumour density ([3]).

Using the notations $\mathbf{c}$, $\mathbf{v}$, $\mathbf{u} \in \mathbb{R}^n$ with $n = n_x n_y$ being the number of mesh points, the system (1) in matrix form after discretization of the space variables becomes

$$\begin{aligned}
\dot{\mathbf{c}}(t) &= D_c \mathbf{G}\mathbf{c}(t) - \mathbf{N}_1(\mathbf{c}(t), \mathbf{u}(t)) - \mathbf{N}_2(\mathbf{c}(t), \mathbf{v}(t)) + \mathbf{N}_3(\mathbf{c}(t), \mathbf{v}(t)), \\
\dot{\mathbf{v}}(t) &= -\mathbf{N}_4(\mathbf{u}(t), \mathbf{v}(t)) + \mathbf{N}_5(\mathbf{c}(t), \mathbf{v}(t)), \\
\dot{\mathbf{u}}(t) &= D_u \mathbf{G}\mathbf{u}(t) + \mathbf{F}_1(\mathbf{c}(t)) + \mathbf{F}_2(\mathbf{u}(t)).
\end{aligned} \tag{2}$$

In (2), $\mathbf{F}_1$, $\mathbf{F}_2 : \mathbb{R}^n \to \mathbb{R}^n$ and $\mathbf{N}_1$, $\mathbf{N}_2$, $\mathbf{N}_3$, $\mathbf{N}_4$, $\mathbf{N}_5 : \mathbb{R}^n \times \mathbb{R}^n \to \mathbb{R}^n$ are

$$\begin{aligned}
&\mathbf{N}_1(\mathbf{c}, \mathbf{u}) = \chi_c(\mathbf{c}. * \mathbf{G}\mathbf{u} + \mathbf{G}_x\mathbf{c}. * \mathbf{G}_x\mathbf{u} + \mathbf{G}_y\mathbf{c}. * \mathbf{G}_y\mathbf{u}), \\
&\mathbf{N}_2(\mathbf{c}, \mathbf{v}) = \xi_c(\mathbf{c}. * \mathbf{G}\mathbf{v} + \mathbf{G}_x\mathbf{c}. * \mathbf{G}_x\mathbf{v} + \mathbf{G}_y\mathbf{c}. * \mathbf{G}_y\mathbf{v}), \\
&\mathbf{N}_3(\mathbf{c}, \mathbf{v}) = \mu_1. * \mathbf{c}(1 - \mathbf{c} - \mathbf{v}),\ \mathbf{N}_4(\mathbf{u}, \mathbf{v}) = \delta\mathbf{u}. * \mathbf{v},\ \mathbf{N}_5(\mathbf{c}, \mathbf{v}) = \mu_2\mathbf{c}. * (1 - \mathbf{c} - \mathbf{v}), \\
&\mathbf{F}_1(\mathbf{c}) = \alpha\mathbf{c}, \quad \mathbf{F}_2(\mathbf{u}) = -\beta\mathbf{u}\,.
\end{aligned}$$

POD-reduced system. We consider the following snapshot matrices for the construction of POD-reduced system: $\widehat{\mathbf{C}} = [\mathbf{c}^1, \ldots, \mathbf{c}^{n_s}]$, $\widehat{\mathbf{V}} = [\mathbf{v}^1, \ldots, \mathbf{v}^{n_s}]$, and $\widehat{\mathbf{U}} = [\mathbf{u}^1, \ldots, \mathbf{u}^{n_s}] \in \mathbb{R}^{n \times n_s}$. Here, $\mathbf{c}^j$, corresponds to the solution of the FD discretized system at time t_j and similarly for $\mathbf{v}^j$, and $\mathbf{u}^j$. Let $r_c = \text{rank}(\widehat{\mathbf{C}})$, $r_v = \text{rank}(\widehat{\mathbf{V}})$, $r_u = \text{rank}(\widehat{\mathbf{U}})$. Let $k \leq \min\{r_c, r_v, r_u\}$. The POD basis of dimension k of the snapshots $\{\mathbf{c}^j\}_{j=1}^{n_s}$ is the set of left singular values and likewise for the snapshots $\{\mathbf{v}^j\}_{j=1}^{n_s}$, $\{\mathbf{u}^j\}_{j=1}^{n_s}$. Hence, the POD basis of the snapshots $\{\mathbf{c}^j\}_{j=1}^{n_s}$ denoted by $\mathbf{A}$ consists of the leading k orthonormal columns of $\widehat{\mathbf{A}}$, $\mathbf{A} = \widehat{\mathbf{A}}(:, 1:k) \in \mathbb{R}^{n \times k}$, where $\widehat{\mathbf{C}} = \widehat{\mathbf{A}}\Sigma^c(\mathbf{Z}^c)^T$ is the SVD of $\widehat{\mathbf{C}}$ with $\widehat{\mathbf{A}} \in \mathbb{R}^{n \times n}$, $\Sigma^c \in \mathbb{R}^{n \times n_s}$ and $\mathbf{Z}^c \in \mathbb{R}^{n_s \times n_s}$. The diagonal entries of Σ^c are the singular values of $\widehat{\mathbf{C}}$. Similarly, let $\mathbf{B}$, $\mathbf{D} \in \mathbb{R}^{n \times k}$ be matrices whose columns corresponding to the POD basis of dimension k of the snapshots $\{\mathbf{v}^j\}_{j=1}^{n_s}$, and $\{\mathbf{u}^j\}_{j=1}^{n_s}$.

The POD reduced-order system is constructed by applying Galerkin projection method on the equations in (2). In particular, replacing the discrete state variables by their truncated POD expansions $\mathbf{c} \leftarrow \mathbf{A}\check{\mathbf{c}}$, $\mathbf{v} \leftarrow \mathbf{B}\tilde{\mathbf{v}}$, $\mathbf{u} \leftarrow \mathbf{D}\tilde{\mathbf{u}}$ with reduced variables $\tilde{\mathbf{c}}$, $\tilde{\mathbf{v}}$, $\tilde{\mathbf{u}} \in \mathbb{R}^k$, and then forcing the Galerkin orthogonality condition of the residuals by pre-multiplying the four equations in (2) by $\mathbf{A}^T$, $\mathbf{B}^T$, and $\mathbf{D}^T$, respectively, we obtain the following reduced-order system

$$\begin{aligned}
\dot{\tilde{\mathbf{c}}}(t) &= D_c \underbrace{\mathbf{A}^T\mathbf{G}\mathbf{A}}_{\mathbf{G}_c}\tilde{\mathbf{c}}(t) - \mathbf{A}^T\tilde{\mathbf{N}}_1(\tilde{\mathbf{c}}(t), \tilde{\mathbf{u}}(t)) \\
&\quad - \mathbf{A}^T\tilde{\mathbf{N}}_2(\tilde{\mathbf{c}}(t), \tilde{\mathbf{v}}(t)) + \mathbf{A}^T\tilde{\mathbf{N}}_3(\tilde{\mathbf{c}}(t), \tilde{\mathbf{v}}(t)), \\
\dot{\tilde{\mathbf{v}}}(t) &= -\mathbf{B}^T\tilde{\mathbf{N}}_4(\tilde{\mathbf{u}}(t), \tilde{\mathbf{v}}(t)) + \mathbf{B}^T\tilde{\mathbf{N}}_5(\tilde{\mathbf{c}}(t), \tilde{\mathbf{v}}(t)), \\
\dot{\tilde{\mathbf{u}}}(t) &= D_u \underbrace{\mathbf{D}^T\mathbf{G}\mathbf{D}}_{\mathbf{G}_u}\tilde{\mathbf{u}}(t) + \mathbf{D}^T\mathbf{F}_1(\mathbf{A}\check{\mathbf{c}}(t)) + \mathbf{D}^T\mathbf{F}_3(\mathbf{D}\tilde{\mathbf{u}}(t)),
\end{aligned} \tag{3}$$

where $\tilde{\mathbf{N}}_1$, $\tilde{\mathbf{N}}_2$, $\tilde{\mathbf{N}}_3$, $\tilde{\mathbf{N}}_4$, $\tilde{\mathbf{N}}_5 : \mathbb{R}^k \times \mathbb{R}^k \to \mathbb{R}^n$ are

$$\begin{aligned}
\tilde{\mathbf{N}}_1(\tilde{\mathbf{c}}, \tilde{\mathbf{u}}) &= \chi_c(\tilde{\mathbf{c}}. * \mathbf{A}^T\mathbf{G}\mathbf{B}\tilde{\mathbf{u}} + \mathbf{A}^T\mathbf{G}_x\mathbf{A}\tilde{\mathbf{c}}. * \mathbf{A}^T\mathbf{G}_x\mathbf{B}\tilde{\mathbf{u}} + \mathbf{A}^T\mathbf{G}_y\mathbf{A}\tilde{\mathbf{c}}. * \mathbf{A}^T\mathbf{G}_y\mathbf{B}\tilde{\mathbf{u}}),\\
\tilde{\mathbf{N}}_2(\tilde{\mathbf{c}}, \tilde{\mathbf{v}}) &= \xi_c(\tilde{\mathbf{c}}. * \mathbf{A}^T\mathbf{G}\mathbf{B}\tilde{\mathbf{v}} + \mathbf{A}^T\mathbf{G}_x\mathbf{A}\tilde{\mathbf{c}}. * \mathbf{A}^T\mathbf{G}_x\mathbf{B}\tilde{\mathbf{v}} + \mathbf{A}^T\mathbf{G}_y\mathbf{A}\tilde{\mathbf{c}}. * \mathbf{A}^T\mathbf{G}_y\mathbf{B}\tilde{\mathbf{v}}),\\
\tilde{\mathbf{N}}_3(\tilde{\mathbf{c}}, \tilde{\mathbf{v}}) &= \mu_1\tilde{\mathbf{c}}. * (1 - \tilde{\mathbf{c}} - \tilde{\mathbf{v}}), \qquad \tilde{\mathbf{N}}_4(\tilde{\mathbf{u}}, \tilde{\mathbf{v}}) = \delta\tilde{\mathbf{u}}. * \tilde{\mathbf{v}},\\
\tilde{\mathbf{N}}_5(\tilde{\mathbf{c}}, \tilde{\mathbf{v}}) &= \mu_2\tilde{\mathbf{v}}. * (1 - \tilde{\mathbf{c}} - \tilde{\mathbf{v}}).
\end{aligned}$$

Let $\mathbf{f} : \mathcal{D} \mapsto \mathbb{R}^n$ be o nonlinear vector-valued function with $\mathcal{D} \subset \mathbb{R}^d$, for some positive integer d. Let $\{\mathbf{S}\}_{\ell=1}^m \subset \mathbb{R}^n$ be a linearly independent set, for $m = 1, \ldots, n$. For $\tau \in \mathcal{D}$, the DEIM approximation of order m for $\mathbf{f}(\tau)$ in the space spanned by $\{\mathbf{S}\}_{\ell=1}^m$ is given (see [4]) by $\widehat{\mathbf{f}}(\tau) := \mathbf{S}(\mathbf{P}^T\mathbf{S})^{-1}\mathbf{P}^T\mathbf{f}(\tau)$, where $\mathbf{S} = [\mathbf{S}_1, \ldots, \mathbf{S}_m] \in \mathbb{R}^{n\times m}$ collects the first m POD basis modes of nonlinear function $\mathbf{f}$ and $\mathbf{P} = [\mathbf{e}_{\varrho_1}, \ldots, \mathbf{e}_{\varrho_m}] \in \mathbb{R}^{n\times m}$ is the DEIM interpolation selection matrix. The DEIM procedure employs a greedy technique and iteratively constructs a set of indices $\{\varrho_1, \ldots, \varrho_m\}$ using the input basis $\{\mathbf{S}_i\}_{i=1}^m$, in such a way that, at each iteration, the current selected index captures the maximum variation of the input basis vectors (see [1],[4]).

POD-DEIM reduced system. Let $\mathbf{S}^{N_1}$, $\mathbf{S}^{N_2}$, $\mathbf{S}^{N_3}$, $\mathbf{S}^{N_4}$, $\mathbf{S}^{N_5} \in \mathbb{R}^{n\times m}$, $m \le n$ be the matrices whose columns containing the POD basis of the nonlinear functions $\tilde{\mathbf{N}}_1$, $\tilde{\mathbf{N}}_2$, $\tilde{\mathbf{N}}_3$, $\tilde{\mathbf{N}}_4$, and $\tilde{\mathbf{N}}_5$ respectively, defined in (3). These POD bases are used to select the sets of m interpolation indices from DEIM algorithm. Let $\vec{\varrho}^{N_1}$, $\vec{\varrho}^{N_2}$, $\vec{\varrho}^{N_3}$, $\vec{\varrho}^{N_4}$, $\vec{\varrho}^{N_5}$ be the DEIM interpolation indices of the nonlinear functions defined in (3). Let $\mathbf{P}_{N_1} \in \mathbb{R}^{n\times m}$ be the matrix whose j-th column is the $\varrho_j^{N_1}$-th column of the identity matrix, i.e., it is the vector $[0, \ldots, 0, 1, 0, \ldots, 0]^T \in \mathbb{R}^n$, having all zeros entries except one at the entry $\varrho_j^{N_1}$, for $j = 1, \ldots, m$. Define $\mathbf{P}_{N_2}$, $\mathbf{P}_{N_3}$, $\mathbf{P}_{N_4}$, $\mathbf{P}_{N_5} \in \mathbb{R}^{n\times m}$ in a similar way as $\mathbf{P}_{N_1}$. The DEIM approximation of the nonlinear functions in (3) is

$$\begin{aligned}
\tilde{\mathbf{N}}_1 &\approx \mathbf{S}^{N_1}(\mathbf{P}_{N_1}^T\mathbf{S}^{N_1})^{-1}\tilde{\mathbf{N}}_1^m, \qquad \tilde{\mathbf{N}}_2 \approx \mathbf{S}^{N_2}(\mathbf{P}_{N_2}^T\mathbf{S}^{N_2})^{-1}\tilde{\mathbf{N}}_2^m,\\
\tilde{\mathbf{N}}_3 &\approx \mathbf{S}^{N_3}(\mathbf{P}_{N_3}^T\mathbf{S}^{N_3})^{-1}\tilde{\mathbf{N}}_3^m, \qquad \tilde{\mathbf{N}}_4 \approx \mathbf{S}^{N_4}(\mathbf{P}_{N_4}^T\mathbf{S}^{N_4})^{-1}\tilde{\mathbf{N}}_4^m,\\
\tilde{\mathbf{N}}_5 &\approx \mathbf{S}^{N_5}(\mathbf{P}_{N_5}^T\mathbf{S}^{N_5})^{-1}\tilde{\mathbf{N}}_5^m,
\end{aligned} \tag{4}$$

and the nonlinear terms for the POD reduced system can be approximated as

$$\mathbf{A}^T\tilde{\mathbf{N}}_1(\tilde{\mathbf{c}}, \tilde{\mathbf{v}}) \approx \underbrace{\mathbf{A}^T\mathbf{S}^{N_1}(\mathbf{S}_{\vec{\varrho}}^{N_1})^{-1}}_{E_1}\tilde{\mathbf{N}}_1^m, \quad \mathbf{A}^T\tilde{\mathbf{N}}_2(\tilde{\mathbf{u}}, \tilde{\mathbf{w}}) \approx \underbrace{\mathbf{A}^T\mathbf{S}^{N_2}(\mathbf{S}_{\vec{\varrho}}^{N_2})^{-1}}_{E_2}\tilde{\mathbf{N}}_2^m,$$

$$\mathbf{A}^T\tilde{\mathbf{N}}_3(\tilde{\mathbf{v}}, \tilde{\mathbf{h}}) \approx \underbrace{\mathbf{A}^T\mathbf{S}^{N_3}(\mathbf{S}_{\vec{\varrho}}^{N_3})^{-1}}_{E_3}\tilde{\mathbf{N}}_3^m, \quad \mathbf{B}^T\tilde{\mathbf{N}}_4(\tilde{\mathbf{u}}, \tilde{\mathbf{w}}) \approx \underbrace{\mathbf{B}^T\mathbf{S}^{N_4}(\mathbf{S}_{\vec{\varrho}}^{N_4})^{-1}}_{E_4}\tilde{\mathbf{N}}_4^m,$$

$$\mathbf{B}^T\tilde{\mathbf{N}}_5(\tilde{\mathbf{c}}, \tilde{\mathbf{v}}) \approx \underbrace{\mathbf{B}^T\mathbf{S}^{N_5}(\mathbf{S}_{\vec{\varrho}}^{N_5})^{-1}}_{E_5}\tilde{\mathbf{N}}_5^m,$$

where the nonlinear functions $\tilde{\mathbf{N}}_1^m$, $\tilde{\mathbf{N}}_2^m$, $\tilde{\mathbf{N}}_3^m$, $\tilde{\mathbf{N}}_4^m$, $\tilde{\mathbf{N}}_5^m : \mathbb{R}^k \times \mathbb{R}^k \to \mathbb{R}^m$ are defined as:

$$\begin{aligned}
&\tilde{\mathbf{N}}_1^m(\tilde{\mathbf{c}}, \tilde{\mathbf{u}}) = \mathbf{P}_{N_1}^T \tilde{\mathbf{N}}_1(\tilde{\mathbf{c}}, \tilde{\mathbf{u}}) \qquad && \tilde{\mathbf{N}}_2^m(\tilde{\mathbf{c}}, \tilde{\mathbf{v}}) = \mathbf{P}_{N_2}^T \tilde{\mathbf{N}}_2(\tilde{\mathbf{c}}, \tilde{\mathbf{v}}), \\
&\tilde{\mathbf{N}}_3^m(\tilde{\mathbf{c}}, \tilde{\mathbf{v}}) = \mathbf{P}_{N_3}^T \tilde{\mathbf{N}}_3(\tilde{\mathbf{c}}, \tilde{\mathbf{v}}), \qquad && \tilde{\mathbf{N}}_4^m(\tilde{\mathbf{u}}, \tilde{\mathbf{v}}) = \mathbf{P}_{N_4}^T \tilde{\mathbf{N}}_4(\tilde{\mathbf{u}}, \tilde{\mathbf{v}}), \\
&\tilde{\mathbf{N}}_5^m(\tilde{\mathbf{c}}, \tilde{\mathbf{v}}) = \mathbf{P}_{N_5}^T \tilde{\mathbf{N}}_5(\tilde{\mathbf{c}}, \tilde{\mathbf{v}}).
\end{aligned} \tag{5}$$

The explicit form of $\tilde{\mathbf{N}}_1^m(\tilde{\mathbf{c}}, \tilde{\mathbf{u}})$ is given by

$$\begin{aligned}
= \chi_c[&(\underbrace{\mathbf{P}_{N_1}^T \mathbf{A}}\, \tilde{\mathbf{c}}) .* (\underbrace{\mathbf{P}_{N_1}^T \mathbf{G} \mathbf{D}}\, \tilde{\mathbf{u}}) + (\underbrace{\mathbf{P}_{N_1}^T \mathbf{G}_x \mathbf{A}}\, \tilde{\mathbf{c}}) .* (\underbrace{\mathbf{P}_{N_1}^T \mathbf{G}_x \mathbf{D}}\, \tilde{\mathbf{u}}) \\
&+ (\underbrace{\mathbf{P}_{N_1}^T \mathbf{G}_y \mathbf{A}}\, \tilde{\mathbf{c}}) .* (\underbrace{\mathbf{P}_{N_1}^T \mathbf{G}_y \mathbf{D}}\, \tilde{\mathbf{u}})]
\end{aligned} \tag{6}$$

and similarly for $\tilde{\mathbf{N}}_2^m$, $\tilde{\mathbf{N}}_3^m$, $\tilde{\mathbf{N}}_4^m$, $\tilde{\mathbf{N}}_5^m$. We remark that the k-by-m matrices

$$\begin{aligned}
&\mathbf{E}_1 = \mathbf{A}^T \mathbf{S}^{N_1} (\mathbf{S}_{\vec{\varrho}}^{N_1})^{-1}, \qquad \mathbf{E}_2 = \mathbf{A}^T \mathbf{S}^{N_2} (\mathbf{S}_{\vec{\varrho}}^{N_2})^{-1}, \qquad \mathbf{E}_3 = \mathbf{A}^T \mathbf{S}^{N_3} (\mathbf{S}_{\vec{\varrho}}^{N_3})^{-1}, \\
&\mathbf{E}_4 = \mathbf{B}^T \mathbf{S}^{N_4} (\mathbf{S}_{\vec{\varrho}}^{N_4})^{-1}, \qquad \mathbf{E}_5 = \mathbf{B}^T \mathbf{S}^{N_5} (\mathbf{S}_{\vec{\varrho}}^{N_5})^{-1}
\end{aligned}$$

can be precomputed and reused at each time step. Also, each of the m-by-k coefficient matrices in (6) grouped by the curly brackets are precomputed so that the computational complexity of each nonlinear function is independent of the dimension n of the original full-order system. Using the coefficient matrices in (3) the form of the POD-DEIM reduced system becomes

$$\begin{aligned}
&\dot{\tilde{\mathbf{c}}}(t) = D_c \mathbf{G}_u \tilde{\mathbf{c}}(t) - \mathbf{E}_1 \tilde{\mathbf{N}}_1^m(\tilde{\mathbf{c}}(t), \tilde{\mathbf{u}}(t)) - \mathbf{E}_2 \tilde{\mathbf{N}}_2^m(\tilde{\mathbf{c}}(t), \tilde{\mathbf{v}}(t)) + \mathbf{E}_3 \tilde{\mathbf{N}}_3^m(\tilde{\mathbf{c}}(t), \tilde{\mathbf{v}}(t)), \\
&\dot{\tilde{\mathbf{v}}}(t) = -\mathbf{E}_4 \tilde{\mathbf{N}}_4^m(\tilde{\mathbf{u}}(t), \tilde{\mathbf{v}}(t)) + \mathbf{E}_5 \tilde{\mathbf{N}}_5^m(\tilde{\mathbf{c}}(t), \tilde{\mathbf{v}}(t)), \\
&\dot{\tilde{\mathbf{u}}}(t) = D_u \mathbf{G}_w \tilde{\mathbf{u}}(t) + \mathbf{D}^T \mathbf{F}_1(\mathbf{C}\tilde{\mathbf{c}}(t)) + \mathbf{D}^T \mathbf{F}_2(\mathbf{D}\tilde{\mathbf{u}}(t)).
\end{aligned}$$

Numerical simulations indicate that DEIM improves the efficiency of the POD approximation and achieves a complexity reduction of the nonlinear terms.

References

[1] Barrault, M., Maday, Y., Nguyen, N.C., Patera, A.T., An "empirical interpolation" method: application to efficient reduced-basis discretization of partial differential equations, *C.R. Math. Acad. Sci. Paris*, **339** (2004) 667–672 .

[2] Chaplain, M.A.J., Lolas, G., Mathematical Modelling of Cancer Cell Invasion of Tissue: The Role of The Urokinase Plasminogen Activation System, *Mathematical Models and Methods in Applied Sciences*, **15** (2005) 1685–1734.

[3] Chaplain, M.A.J., Lolas, G., Mathematical modelling of cancer invasion of tissue: Dynamic heterogeneity, *Netw. Heterog. Media*, **1** (3) (2006) 399–439.

[4] Chaturantabut, S., Sorensen, D.C., Discrete Empirical Interpolation for Nonlinear Model Reduction, TR09–05, CAAM, Rice University (2009).

Analysis and Realization of Compact Difference Schemes for Semilinear Parabolic Systems

I. Dimov, J. Kandilarov, V. Todorov, L. Vulkov

1 Introduction

In this work we construct compact finite high-order difference schemes (CFDS) for parabolic systems and propose fast algorithms for solution of the nonlinear algebraic equations. Problems of air pollution transport with coupling in the nonlinear reactions terms are of our main consideration, namely,

$$\partial u_s/\partial t - K\triangle u_s + \mathbf{b_s}.\nabla u_s + R_s(x, y, u_1, \ldots, u_S) = 0, \quad u_s|_{\partial\Omega\times R^+} = 0, \qquad (1)$$

where $u_s = u_s(x, y, t)$ are the concentrations of S chemical species (pollutants) and $K > 0$ is the diffusion coefficient. The assumption of constant $K := K_x = K_y$ is not a restriction, but just corresponds to the physical model described in [1, 2, 3]. The error estimate shows the fourth order accuracy of the proposed CFDS when two spatial mesh sizes are proportional. For time discretization θ-weight method combined with inexact Newton iterations is implemented. Also, three implicit-explicit (IMEX) time discrete methods, namely IMEX-BDF1, IMEX-BDF2 and CN-LF are developed for the ODE-s systems arising after the space discretization. Another possible approach is discussed in ([4]). We illustrate a high efficiency of the computational algorithms when they are used to model air pollution transport.

2 Difference schemes

We start with presenting CFDS on the 1D system of the following two equations:

$$\frac{\partial u}{\partial t} - a(x)\frac{\partial^2 u}{\partial x^2} + b(x)\frac{\partial u}{\partial x} = f(x, t, u, v), \quad \frac{\partial v}{\partial t} - c(x)\frac{\partial^2 u}{\partial x^2} + d(x)\frac{\partial u}{\partial x} = g(x, t, u, v)\ . \quad (2)$$

We introduce a standard mesh: $\Omega_h = \{x_i = ih, \quad i = 0, 1, \ldots, M, \quad h = 1/M\}$ and the difference operators $\delta_x\varphi_i = (\varphi_{i+1} - \varphi_{i-1})/2h$, $\delta_x^2\varphi_i = (\varphi_{i+1} - 2\varphi_i + \varphi_{i-1})/h^2$ for some mesh function φ_i, $i = 0, 1, \ldots, M$. Applying these operators to the elliptic part of the system one may obtain

$$-a_i\delta_x^2 u_i + b_i\delta_x u_i - e_{1,i} = f(x_i, t, u_i, v_i) - \frac{\partial u_i}{\partial t} \equiv F_i \qquad (3a)$$

$$-c_i\delta_x^2 v_i + d_i\delta_x v_i - e_{2,i} = g(x_i, t, u_i, v_i) - \frac{\partial v_i}{\partial t} \equiv G_i, \qquad (3b)$$

where the truncation errors may be expressed in the following form:

$$e_{1,i} = \frac{h^2}{12}\left(2b\frac{\partial^3 u}{\partial x^3} - a\frac{\partial^2 u}{\partial x^2}\right)\Big|_i + O(h^4) \quad e_{2,i} = \frac{h^2}{12}\left(2d\frac{\partial^3 v}{\partial x^3} - c\frac{\partial^2 u}{\partial x^2}\right)_i + O(h^4).$$

Differentiating (2) twice with respect to x we obtain

$$\begin{cases} a\frac{\partial^3 u}{\partial x^3} = \left(b - \frac{da}{dx}\right)\frac{\partial^2 u}{\partial x^2} - \frac{db}{dx}.\frac{\partial u}{\partial x} - \frac{\partial F}{\partial x} \\ a\frac{\partial^4 u}{\partial x^4} - 2b\frac{\partial^3 u}{\partial x^3} = \left(2\frac{db}{dx} - \frac{d^2 a}{dx^2}\right)\frac{\partial^2 u}{\partial x^2} + \frac{d^2 b}{\partial x^2}\frac{\partial u}{\partial x} - \left(b + 2\frac{da}{dx}\right)\frac{\partial^3 u}{\partial x^3} - \frac{\partial^2 F}{\partial x^2}. \end{cases}$$

To increase the order of the error to $O(h^4)$ in (3a) we have used the fact that

$$\begin{aligned} \left(a\frac{\partial^4 u}{\partial x^4} - 2b\frac{\partial^3 u}{\partial x^3}\right)_i = & - (\delta_x^2 a_i - \widetilde{a}_i(\delta_x a_i - b_i) - 2\delta_x b_i)\delta_x^2 u_i \\ & + (\delta_x b_i - \widetilde{a}_i.\delta_x c_i)\delta_x u_i - \delta_x^2 F_i + \widetilde{a}_i F_i + O(h^2), \end{aligned}$$

where $\widetilde{a}_i = (b_i + 2\delta_x a_i)/a_i \quad i = 1, \ldots, M-1$. Let $\alpha_i = (\delta_x^2 a_i - \widetilde{a}_i(\delta_x a_i - b_i) - 2\delta_x b_i)$, $\widetilde{\alpha}_i = a_i + \frac{h^2}{12}\alpha_i$, $\widetilde{\widetilde{\alpha}}_i = b_i + \frac{h^2}{12}(\delta_x^2 b_i - \widetilde{a}_i \delta_i b_i)$. Now, let us define the following difference operators:

$$l_i^h = -\widetilde{\alpha}_i\delta_x^2 + \widetilde{\widetilde{\alpha}}_i\,\delta_x, \quad \nu_i^h = 1 + \frac{h^2}{12}(\delta_x^2 - \widetilde{a}_i\delta_x), \quad \mathcal{P}_i^h = 6h^2 l_i^h, \quad \mathcal{Q}_i^h = 6h^2\nu_i^h\ .$$

Let also $P_1 = tridiag(p_{i,i-1}, p_{i,i}, p_{i,i+1})$ and $Q_1 = tridiag(q_{i,i-1}, q_{i,i}, q_{i,i+1})$ be three-diagonal matrix corresponding to $\mathcal{P}$, $\mathcal{Q}$ with elements $p_{i,i} = 12a_i + h^2\alpha$, $p_{i,i\pm1} = -6a_i \pm \widetilde{\alpha}_i - 0.5h^2\alpha$, $q_{ii} = 5h^2 \quad q_{i,i\pm1} = 0.25h^2(2 \mp \widetilde{\alpha}_i h)$. Finally, if $U_i \approx u(x_i, t)$, then the semidiscretization of (3a) to order $O(h^4)$ is as follows:

$$\mathcal{P}_i^h U_i = \mathcal{Q}^h F_i \ \ i = 1, \ldots, M-1 \ \text{ and } \ U_0 = \Psi(x_0) \ \ U_M = \Psi(x_M). \tag{4}$$

In a similar way we treat (3b). Analoguous to $\widetilde{a}_i$, α_i, $\widetilde{\alpha}_i$, $\widetilde{\widetilde{\alpha}}_i$, P_1 and Q_1 we define $\widetilde{c}_i$, β_i, $\widetilde{\beta}_i$, $\widetilde{\widetilde{\beta}}_i$, P_2 and Q_2, replacing $a \leftrightarrow c$ and $b \leftrightarrow d$.

3 Time discretization

The ODE system (4) is rewritten in a canonical form

$$\frac{\partial U}{\partial t} = L_1 U + f(U, V) \qquad \frac{\partial V}{\partial t} = L_2 U + g(U, V)\ , \tag{5}$$

where $L_1 = Q_1^{-1}P_1$, $L_2 = Q_2^{-1}P_2$ and $U = (U_0, U_1, \ldots, U_M)^T$, $V = (V_0, V_1, \ldots, V_M)^T$, $f(U, V) = (f(U_0, V_0), f(U_1, V_1), \ldots f(U_{M+1}, V_{M+1}))^T$. In this section we study the stability, consistency and convergence of implicit-explicit (IMEX) time discretization methods. Let $\Omega_\tau = \{t_j = j\tau, \ \ j = 0, 1, \ldots, N, \ \ \tau = T/N\}$ be uniform mesh in time. For the full discretization we consider the following cases:

1. *Weight θ-discretization*

$$\frac{U^{j+1} - U^j}{\tau} = (L_1 U)^{j,\theta} + (f(U, V))^{j,\theta}, \ \frac{V^{j+1} - V^j}{\tau} = (L_2 V)^{j,\theta} + (g(U, V))^{j,\theta}, \tag{6}$$

where $W^{j,\theta} = \theta W^{j+1} + (1-\theta)W^j$, $0 \le \theta \le 1$.

2. *IMEX - BDF1 (IMEX backward difference method of order one)*

$$U^0(x)=\varphi(x),\quad V^0(x)=\psi(x)\qquad \varphi(x),\psi(x)\text{-given},$$
$$\frac{U^{j+1}-U^j}{\tau}=L_1U^{j+1}+f(U^j,V^j),\qquad \frac{V^{j+1}-V^j}{\tau}=L_2V^{j+1}+g(U^j,V^j).$$

3. *IMEX - BDF2 (IMEX backward difference method of second order)*

$U^j(x)$, $V^j(x)$ for $j=0,1$ equal to these computed by IMEX - BDF1 and

$$\begin{aligned}\frac{3/2U^{j+1}-2U^j+1/2U^{j-1}}{2\tau} &= L_1(\frac{U^{j+1}+U^{j-1}}{2})+f(U^j,V^j)\ ,\\ \frac{3/2V^{j+1}-2V^j+1/2V^{j-1}}{2\tau} &= L_2(\frac{V^{j+1}+V^{j-1}}{2})+g(U^j,V^j)\ .\end{aligned}$$

4. *CN-LF (Crank-Nicolson Leap Frog)*

$$\begin{aligned}\frac{U^{j+1}-U^{j-1}}{2\tau} &= L_1(\frac{U^{j+1}+U^{j-1}}{2})+f(U^j,V^j)\ ,\\ \frac{V^{j+1}-V^{j-1}}{2\tau} &= L_2(\frac{V^{j+1}+V^{j-1}}{2})+g(U^j,V^j)\ .\end{aligned}$$

We have shown that IMEX-BDF2 and CN-LF are stable and second order accurate in time, whereas IMEX-BDF1 is stable but only first order accurate.

4 Algorithms for solution of difference equations

This section is concerned with the computational algorithms for the finite difference systems that arise after the discretizations described in Sections 2,3. The methods 2-4 are easy for implementation (one only have to solve three-diagonal system of algebraic equations), while the method 1 for $\theta>0$ requires solving of nonlinear algebraic systems. We briefly discuss the application of the Newton method on the problem (2). To apply the classical Newton method the system (5) is rewritten in the form $\Phi(\widehat{W})=0$, where $\widehat{W}=[\widehat{U},\widehat{V}]$ is a vector of length $2(M+1)$. We set $\widehat{W}^0$ to be the numerical solution on the previous time layer $t=t_j$. Then to find the solution on $t=t_{j+1}$ we use the iterative process with appropriate stopping rule:

$$\Phi'(\widehat{W}^k)s_k=-\Phi(\widehat{W}^k),\quad \widehat{W}^{k+1}=\widehat{W}^k+s_k,\ \ k=0,1,\dots\ .$$

We consider problem (2) with parameters $a=b=c=d=1$, $f(x,t,u,v)=u(1-u-v)+\xi_1(x,t)$, $g=(x,t,u,v)=v(1-u-v)+\xi_2(x,t)$, where functions ξ_1 and ξ_2 are chosen so that the exact solutions is $u=e^{-t}\sin(\pi x)$ and $v=e^{-t}x(1-x)$. The implicit Euler method gives an error of order $O(h^4+\tau)$ and this leads to increasing of the number of the time layers. So we use also Crank-Nicolson method for the standard $O(h^2+\tau^2)$ scheme and compact scheme which is $O(h^4+\tau^2)$. The results are presented

in Table 1. With err_N we denote the error in maximum norm on the last time layer $t_j = T$ $err_N = \max_i |U_i^N - u(x_i, T)|$. The $ratio = err_N/err_{2N}$ and corresponding CPU time are also produced. The results confirm convergence of fourth order of the CFDS and the theoretical investigations. The advantage of the proposed numerical method is clearly seen from the higher accuracy and the shorter CPU time.

Table 1: The errors in maximum norm for the numerical example

Standard scheme $O(h^2 + \tau^2)$					Compact scheme $O(h^4 + \tau^2)$				
M	N	err_N	ratio	CPU	M	N	error	ratio	CPU
10	10	3.82 e-03		0.36	10	40	1.36 e-05	-	0.473
20	20	9.11 e-04	4.19	0.94	20	160	8.34 e-07	18.5	1.503
40	40	2.23 e-04	4.08	3.49	40	640	5.19 e-08	16.1	5.354
80	80	5.51 e-05	4.05	8.71	80	2560	3.24 e-09	16.02	25.98
160	160	1.37 e-05	4.02	25					

Acknowledgement. This work was partially supported by the Bulgarian National Science Fund under the grant DFNI I-20/2014, as well as by the Bulgarian Academy of Sciences through the "Young Scientists" Grant No. DFNP-91/04.05.2016.

References

[1] J. Karatson, T. Kurics. A preconditioned iterative solution scheme for nonlinear parabolic systems arizing in air pollution modeling. Math. Mod. Anal. 18 (5)(2013) 641-653

[2] K. Georgiev, Z. Zlatev. Implementation of sparse matrix algorithms in an advection-diffusion-chemistry model. J. of Comp. Appl. Math., 236 (3) (2011) 342-353

[3] Z. Zlatev, I. Dimov. Computational and Numerical Challenges in Air Polution Modelling. Elsevier Science (2006)

[4] Z. Zlatev, I. Dimov, I. Farago, K. Georgiev, and A. Havasi. Application of Richardson extrapolation for multi-dimensional advection equations, Comp. Math. Appl., V.67 (2014) 2279-2293

InterCriteria Analysis of Different Metaheuristics Applied to E.coli Cultivation Process

Stefka Fidanova,Olympia Roeva

1 Introduction

The InterCriteria Analysis (ICrA) is developed with the goal to receive additional insight into the nature of the criteria involved and discover on this basis existing relations between the criteria themselves [2]. It is based on the apparatus of the Index Matrices (IM) [3, 4], and the Intuitionistic Fuzzy Sets [5] and can be applied for decision making in different areas of knowledge. The approach has been discussed in a number of papers considering parameter estimation problems. In [7] ICrA has been applied for the first time in the field of parameter identification of fermentation processes (FP) models. The ICrA implementation allowed to establish relations and dependencies between two of the main genetic algorithms (GA) parameters âĂŞ numbers of individuals and number of generations, and convergence time, model accuracy and model parameters. In [6] ICrA is applied to find fundamental correlation between the kinetic variables of fed-batch processes for *E. coli* fermentation. In [12] ICrA is applied to determine relations and dependencies between different model parameters. FP of bacteria *E. coli* and yeast *S. cerevisiae* are examined and six different GA are applied for the parameter identification. Further, ICrA is applied to explore the existing relations and dependencies of defined model parameters and GA outcomes âĂŞ- execution time and objective function value âĂŞ- in case of *S. cerevisiae* FP [1] and *E. coli* FP [10]. Moreover, ICrA is applied for establishing the relations and dependencies between GAs parameter generation gap and convergence time, model accuracy and model parameters in case of *E. coli* FP [11] and *S. cerevisiae* FP [8]. Finally ICrA is applied to define the relations and dependencies of considered parameters based on different criteria referred to various metaheuristic algorithms, namely hybrid schemes using GA and Ant Colony Optimization (ACO) [9].

Results of these applications of the ICrA proved that in the case of modelling FP ICrA approach could be very useful. FP are characterized with intricate, non-linear dynamic and their modelling is a hard combinatorial optimization problem. The parameter identification is of high importance for modelling process and additional knowledge about the model parameters relations will be extremely useful to improve the model accuracy. The information may be used to improve the performance of the used optimization algorithms. Thus, the relations between model parameters and optimization algorithm performance will be established.

Encouraging results of these first applications of the ICrA provoke us to use the method for identifying the relations between parameters of the mathematical model of an *E. coli* fed-batch cultivation process. The model parameters are further considered as criteria in terms of ICrA.

In this paper we applied the ICrA to establish the basic relations between the parameters in the model of an *E. coli* fed-batch FP. The existing relations are identified based on results of a series of parameters identification procedures. The use of meta-heuristic techniques such as ACO, GA, Bat Algorithm (BA), Fire Fly algorithm (FF), Tabue Search (TS) and Simulated Annealing (SA), has received more and more attention, therefore our research is focused on them.
Based on ICrA the obtained results are examined and discussion and conclusions about existing relations and dependences between model parameters of the E.coli process and algorithm parameters will be done.

2 Problem Formulation

Let us use the following non-linear differential equation system to describe the *E. coli* fed-batch FP [13]:

$$\frac{dX}{dt} = \mu X - \frac{F_{in}}{V} X, \tag{1}$$

$$\frac{dS}{dt} = -q_S X + \frac{F_{in}}{V}(S_{in} - S), \tag{2}$$

$$\frac{dV}{dt} = F_{in}, \tag{3}$$

where

$$\mu = \mu_{max} \frac{S}{k_S + S}, \;\; q_S = \frac{1}{Y_{S/X}} \mu \tag{4}$$

and X is the biomass concentration, [g/l]; S is the substrate concentration, [g/l]; F_{in} is the feeding rate, [l/h]; V is the bioreactor volume, [l]; S_{in} is the substrate concentration in the feeding solution, [g/l]; μ and q_S are the specific rate functions, [1/h]; μ_{max} is the maximum value of the μ, [1/h]; k_S is the saturation constant, [g/l]; $Y_{S/X}$ is the yield coefficient, [-].
For the model (Eq. (1)-Eq. (4)) the parameters that will be identified are μ_{max}, k_S and $Y_{S/X}$.
Let $Z_{mod} \stackrel{\text{def}}{=} [X_{mod}\ S_{mod}]$ (model predictions for biomass and substrate) and $Z_{exp} \stackrel{\text{def}}{=} [X_{exp}\ S_{exp}]$ (known experimental data for biomass and substrate). Then putting $Z = Z_{mod} - Z_{exp}$, the objective function is defined as:

$$J = \|Z\|^2 \to \min, \tag{5}$$

where $\|\|$ denotes the ℓ^2-vector norm [11].
For the model parameters identification we use experimental data for biomass and glucose concentration of an *E. coli* MC4110 fed-batch fermentation process.

3 InterCriteria Analysis

Following [2] and [5] we will obtain an Intuitionistic Fuzzy Pair (IFP) [5] as the degrees of "agreement" and "disagreement" between two criteria applied on different objects. We remind briefly that an IFP is an ordered pair of real non-negative numbers $\langle a, b\rangle$ such that:

$$a + b \leq 1.$$

Let us be given an Index Matrix (IM)(see [3]) whose index sets consist of the names of the criteria (for rows) and objects (for columns). The elements of this IM are further supposed to be real numbers. We will obtain an IM with index sets consisting of the names of the criteria (for rows and for columns) with elements IFPs corresponding to the "agreement" and "disagreement" of the respective criteria.
Two things are further supposed:

1. All criteria provide an evaluation for all objects (i.e. there are no inapplicable criteria for a given object) and all these evaluations are available (no missing evaluations).

2. All the evaluations of a given criteria can be compared amongst themselves.

Then when comparing two criteria we determine the "degree of agreement" between the two as the number of matching components (divided by the length of the vector for normalization purposes). This can be done in several ways, e.g. by counting the matches or by taking the complement of the Hamming distance. The "degree of disagreement" is the number of components of opposing signs in the two vectors (again normalized by the length). This also may be done in various ways.
In our study there are 5 criteria, the value of the three problem parameters (μ_{max}, k_S, $Y_{S/X}$), the value of the objective function and the execution time. The objects are the six proposed methods to solve the problem, ACO, GA, BA, FF, TS, SA. With this study we find relations between the algorithms performance and their correctness.

Acknowledgment

Work presented here is partially supported by the Bulgarian National Scientific Fund under Grant DFNI-I02/5 âĂIJInterCriteria Analysis. A New Approach to Decision MakingâĂİ and DFNI I02/20 âĂIJEfficient Parallel Algorithms for Large Scale Computational ProblemsâĂİ.

References

[1] M. Angelova, O. Roeva and T. Pencheva, "InterCriteria Analysis of Crossover and Mutation Rates Relations in Simple Genetic Algorithm", *Annals of Computer Science and Information Systems*, Vol. 5, 2015, pp. 419–424.

[2] K. Atanassov, D. Mavrov and V. Atanassova, "Intercriteria Decision Making: A New Approach for Multicriteria Decision Making, Based on Index Matrices and Intuitionistic Fuzzy Sets", *Issues in IFSs and GNs*, Vol. 11, 2014, pp. 1–8

[3] K. Atanassov," On index matrices, Part 1: Standard cases", *Advanced Studies in Contemporary Mathematics*, Vol. 20, 2010, No. 2, pp. 291–302.

[4] K. Atanassov, "On index matrices, Part 2: Intuitionistic fuzzy case", *Proceedings of the Jangjeon Mathematical Society*, Vol. 13, 2010, No. 2, pp. 121–126.

[5] K. Atanassov, *On Intuitionistic Fuzzy Sets Theory*, Springer, Berlin, 2012.

[6] T. Ilkova and M. Petrov, "Intercriteria analysis for identification of *Escherichia coli* fed-batch mathematical model", *J. of Int. Scientific Publications: Materials, Methods & Technology*, Vol. 9, 2015, pp. 598–608.

[7] T. Pencheva , M. Angelova, V. Atanassova and O. Roeva, "InterCriteria Analysis of Genetic Algorithm Parameters in Parameter Identification", *Notes on Intuitionistic Fuzzy Sets*, Vol. 21, 2015, No. 2, pp. 99–110.

[8] T. Pencheva, M. Angelova, P. Vassilev and O. Roeva, "InterCriteria Analysis Approach to Parameter Identification of a Fermentation Process Model", *Advances in Intelligent Systems and Computing*, Vol. 401, 2016, pp. 385–397.

[9] O. Roeva, S. Fidanova and M. Paprzycki, "InterCriteria Analysis of ACO and GA Hybrid Algorithms", *Studies in Computational Intelligence*, Vol. 610, 2016, pp. 107–126.

[10] O. Roeva, S. Fidanova, P. Vassilev and P. Gepner, "InterCriteria Analysis of a Model Parameters Identification using Genetic Algorithm", *Annals of Computer Science and Information Systems*, Vol. 5, 2015, pp. 501–506.

[11] O. Roeva and P. Vassilev, "InterCriteria Analysis of Generation Gap Influence on Genetic Algorithms Performance", *Advances in Intelligent Systems and Computing*, Vol. 401, 2016, pp. 301–313.

[12] O. Roeva, P. Vassilev, M. Angelova and T. Pencheva, "InterCriteria Analysis of Parameters Relations in Fermentation Processes Models", *Lecture Notes in Computer Science*, Vol. 9330, 2015, pp. 171–181.

[13] Roeva, O., Pencheva, T., Hitzmann, B. and Tzonkov, St. (2004) 'A Genetic Algorithms based Approach for Identification of *Escherichia coli* Fed-batch Fermentation', *International Journal Bioautomation*, Vol. 1, pp.30–41.

Some numerical experiments about advection-diffusion problems using finite differences

Mihail Galabov

1 Introduction

This work contains numerical experiment about advection–diffusion problem due to the problem of groundwater flow and contaminant transport. The main function investigated here is the concentration of some pollutant distributed in the groundwater. The transformation to a finite differences model using central differences is presented. The partial derivative by time in the mathematical model gives us the opportunity to make steps by the time. The process is non-stationary. The numerical results show the evolution of the process in time starting from some initial distribution.
The specific task reported in this paper is on a numerical model for a dispersion problem with constant tensor of the coefficient of hydrodynamic dispersion and constant number of porosity.

2 The Mathematical Problem

For the range, defined of the two independent variables, time ($\overline{t} \in \lfloor 0, T_c \rfloor$) and space$\overline{x} \in \lfloor 0, L_c \rfloor$), we have the following model:

$$\begin{aligned} \frac{\partial \overline{c}}{\partial \overline{t}} &= \frac{\partial}{\partial \overline{x}}\left(D\frac{\partial \overline{c}}{\partial \overline{x}}\right) \\ \overline{c}(\overline{x},0) &= \overline{f}(\overline{x}) \\ \frac{\partial \overline{c}}{\partial \overline{x}}(0,\overline{t}) &= \frac{\partial \overline{c}}{\partial \overline{x}}(L_c,\overline{t}) = 0, \end{aligned} \tag{1}$$

where $\overline{c}(\overline{c}\overline{t})$ is the concentration of the substantion $[\overline{c}] = \frac{M}{L^2}$, and $[\overline{D}] = \frac{L^2}{T}$ is the coefficient of hydrodynamic dispersion.

3 Dimensionless variables

From now on we will use the following constants and variables:

- L_c – the length of space interval;
- T_c – the characteristic time;
- S_c – the face of the cylindrical surrounding around the x–axis;

- Q_c – the sum of the mass of the substance, whose concentration $\overline{c}$ we investigate, and
- V_c – the characteristic velocity, which has an influence over the coefficient of hydrodynamic dispersion.

For the independent variables $\overline{x}$ and $\overline{t}$ we have the following dimensionless equivalents:

- $$\begin{aligned} x &= \frac{\partial \overline{x}}{L_c} \qquad x \in [0,1]; \\ t &= \frac{\partial \overline{t}}{T_c} \qquad t \in [0,1]; \end{aligned} \tag{2}$$

- $$c = \frac{\partial \overline{c}}{Q_c}.S_c.L_c, \tag{3}$$

  where $Q_c = \int_0^{L_c} \overline{c}.S_c\, doverlinex$ is the whole mass of the substance, whose concentration is being investigated.

- $$D = \frac{\overline{D}}{V_c.L_c}.S_c.L_c \tag{4}$$

  (D is the dimensionless coefficient of hydrodynamic dispersion)

After the appropriate transformations in (1), we have the following dimensionless model:

$$\frac{\partial c}{\partial t} = k_1 \frac{\partial^2 c}{\partial x^2}, \tag{5}$$

where

$$k_1 = D.V.\frac{T_c}{L_c} = \overline{D}\frac{T_c}{L_c^2} = \frac{1}{Pe}$$

is dimensionless constant; $x \in [0,1]$ and $t \in [0,1]$ are the two dimensionless independent variables, and $c(x,t)$ is the dimensionless concentration of the investigated substance, which is the quotient between the concentration at a certain point and the mean concentration for the whole volume. The corresponding boundary conditions of (1) are transformed to

$$\frac{\partial c}{\partial x}(0,t) = \frac{\partial c}{\partial x}(1,t) = 0, \tag{6}$$

and the corresponding initial condition of (1) is transformed to

$$c(x,0) = f(x). \tag{7}$$

Moreover, the following formulas are true:

$$\overline{c} = \frac{Q_c}{S_c.L_c};$$

$$\int_0^{L_c} \overline{c}(\overline{x}) = \frac{Q_c}{S_c};$$

$$\int_0^1 c(x)dx = 1. \tag{8}$$

4 Finite Differences Problem

Let us introduced the usual equidistant two dimensional grid in $\Omega = [0,1] \times [0,1]$, where:

- $(i,k) = (i.\Delta x, k.\Delta t)$;
- $i = 0, 1, \ldots, N; \quad k = 0, 1, \ldots, P;$
- $\Delta x = 1/N \quad \Delta t = 1/P;$
- N is the number of the space intervals and P is the number of the time intervals.

Let us $c_1^k = c(i.\Delta x, k\Delta t)$, where $c(x,t)$ is the dimensionless function of the concentration.
Having the introduced grid of points and using (5), (6) and (7), we have the following finite differences problem:

$$\frac{c_i^k - c_i^{k-1}}{\Delta t} = k_1.\frac{c_{i-1}^k - 2c_i^k + c_{i+1}^k}{(\Delta x)^2} \qquad i = 1, 2, \ldots, N-1, \quad k > 0. \tag{9}$$

The following four–point pattern is used:

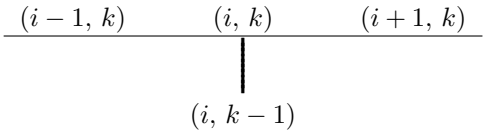

For $i = 0$, $k > 0$, taking into account (6), assuming that $c_(i-1)^k = c_i^k$ and applying (9), we get:

$$\frac{c_i^k - c_i^{k-1}}{\Delta t} = k_1.\frac{-c_i^k + c_{i+1}^k}{(\Delta x)^2} \qquad i = 0, \quad k > 0. \tag{10}$$

The following pattern with not existing left point is used:

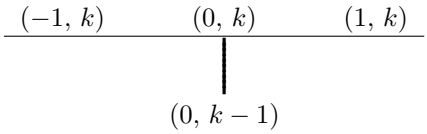

Similarly for the case $i = N$, $k > 0$, we have:

$$\frac{c_i^k - c_i^{k-1}}{\Delta t} = k_1 . \frac{c_{i-1}^k - c_i^k}{(\Delta x)^2} \qquad i = 0, \quad k > 0. \tag{11}$$

The following pattern with not existing right point is used:

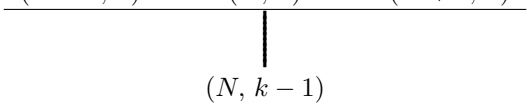

References

[1] K. Liolios, V. Tsihrintzis, K. Moutsopoulos, I. Georgiev, K. Georgiev, *A computational approach for remediation procedures in horizontal subsurface flow constructed wetlands*, Springer, Lecture Notes in Computer Science 7116 (2012) 299-306.

[2] K. Liolios, K. Moutsopoulos, V. Tsihrintzis, *Modelling of flow and BOD fate in horizontal subsurface flow constructed wetlands*, Chemical Engineering Journal 200-2002 (2012) 681-693.

[3] Jacob Bear, Alexander H.-D. Cheng, *Modeling Groundwater Flow and Contaminant Transport*, Springer,Berlin, (2010).

[4] H. K. Versteeg, W. Malalasekera, *Introduction to Computational Fluid Dynamics*, Pearson Education Limited, London, 2007.

Denoising 2D CT Radiographic Images

Stanislav Harizanov, Ivan Lirkov, and Ivan Georgiev

1 Introduction

Accurate 3D *Computed Tomography* (CT) reconstruction of microstructures has numerous applications and is crucial for future realistic numerical simulations of the material's macro characteristics. It is also a quite complicated task, due to the presence of noise in the image. For example, directly segmenting the noisy 3D CT image is not reliable for porous data where standard algorithms may not be able to reconstruct even up to 50% of the material voxel data, thus important quantities (e.g., absolute porosity, average pore size, size and shape of individual pores) which determine its properties are completely miscomputed.
In this short communication, we focus on a single 2D radiographic projection of a CT data. We experimentally verify that Poisson noise indeed appears, has a dominant role in the image noise distribution, and we use the algorithm from [1] for denoising.

2 Poisson-Gaussian noise

To create a radiographic image, the tomograph projects a heterogeneous beam of X-rays towards the object of interest, which is partially absorbed by the object, while the rest is captured behind by a flat panel detector. The gray-scale intensity of each image pixel is proportional to the calculated X-ray amount at the corresponding part of the detector. In such particles-counting processes, errors due to detector's miscalculations inevitably occur. They are statistically modeled by Poisson distribution. If $\bar{u}_i \in \mathbb{N} \cup \{0\}$ is the exact X-ray amount that should be detected at pixel i, the truly detected amount is a realization of a Poisson random variable $f_i = \mathcal{P}(\bar{u}_i)$

$$Pr(f_i = k) = e^{-\bar{u}_i} \frac{\bar{u}_i^k}{k!},$$

with expected value $\bar{u}_i$. On the top of that, there is an additive Gaussian read-out noise $\eta_i \sim \mathcal{N}(0, \sigma^2)$ with zero mean and standard deviation σ, independent of the intensity $\bar{u}_i$. Therefore, the recorded radiographic image u is usually corrupted by a mixed Poisson-Gaussian noise

$$u \sim \mathcal{P}(\bar{u}) + \mathcal{N}(0, \sigma^2). \tag{1}$$

3 Experimental results

We considered a porous geopolymer of cubical shape and, using the industrial tomograph Nikon XT H 225, we recorded a series of radiographic images of fixed position

of the specimen, namely eight single-frame $u_n^{(1)}$ $(n = 1, \dots, 8)$, and one (averaged) 2^n-frame $u_n^{(2)}$ $(n = 1, \dots, 11)$ images. The images are in 8-bit gray-scale bitmap format, meaning that the pixels intensities are integers between 0 and 255. If we assume $\sigma^2 \ll 255$ and that Poisson and Gaussian noise components are independent, we estimate the expected value and variance of (1)

$$E\left(\mathcal{P}(\bar{u}) + \mathcal{N}(0, \sigma^2)\right) = \bar{u}; \quad Var\left(\mathcal{P}(\bar{u}) + \mathcal{N}(0, \sigma^2)\right) = \bar{u} + \sigma^2 \leq 256.$$

Then, the Gaussian noise contribution is negligible and we can use the least-squares Anscombe Transformed algorithm from [1] for image reconstruction. Moreover, applying the *Central Limit Theorem* (CLT) to the 2048-frame image $u_{11}^{(2)}$ we deduct

$$\sqrt{2^{11}}\left(u_{11}^{(2)}(i) - \bar{u}_i\right) \sim \mathcal{N}(0, \bar{u}_i + \sigma^2) \qquad \Longrightarrow$$

$$Pr\left(\left|u_{11}^{(2)}(i) - \bar{u}_i\right| < \frac{1}{2}\right) \geq Pr\left(32\sqrt{2}\left|u_{11}^{(2)}(i) - \bar{u}_i\right| < \sqrt{2}\sqrt{\bar{u}_i + \sigma^2}\right) \approx 84.2\%$$

for every pixel $i = 1, \dots, N$ in the image domain. Due to the 8-bit formatting, the entries of $u_{11}^{(2)}$ are rounded to the closest integer, thus more than 84% of them are expected to coincide with those of $\bar{u}$, while more than 99.73% are expected to be within a unit margin from them. These statistical results were experimentally confirmed, since when two different 2048-frame images were compared we got 76.2% exactness, and 99.85% unit-margin-closeness, respectively. Therefore, $u_{11}^{(2)}$ is a close approximation of the original image $\bar{u}$ and we can use it for quantifying the quality of our denoising process.

In the experiments, we used the constraint

$$\left\| 2\sqrt{v + 3/8} - 2\sqrt{u_n^{(1)} + 3/8} \right\|_2^2 = \#\text{of pixels} =: N$$

for the mathematical model, and we measured PSNR and MAE of the denoised images $v_n^{(1)}$, $n = 1, \dots, 8$ via

$$\text{PSNR} = 10 \log_{10} \frac{\left|\max u_{11}^{(2)} - \min u_{11}^{(2)}\right|^2}{\frac{1}{N}\|v - u_{11}^{(2)}\|_2^2}, \qquad \text{MAE} = \frac{1}{255N}\left\|u_{11}^{(2)} - v\right\|_1.$$

Results are summarized in Table 1. For all the single-frame images $u_n^{(1)}$ we witness similar PSNR and MAE values. Moreover, the least-squares (LSQ) ratio

$$\frac{\left\| 2\sqrt{u_n^{(1)} + 3/8} - 2\sqrt{u_{11}^{(2)} + 3/8} \right\|_2^2}{N} \approx 1, \qquad \forall n = 1, \dots, 8,$$

is also very stable with values almost 1. Both the results strongly support the validity of our assumption on the dominant role of the Poisson noise in the noise distribution and its corollary $u_{11}^{(2)} \approx \bar{u}$. Since $\mathcal{P}(\lambda) + \mathcal{P}(\lambda) \sim \mathcal{P}(2\lambda)$ and LSQ is practically 1-homogeneous (the fraction 3/8 plays no role for large enough gray-scale intensities), as long as the Poisson noise remains dominant, the LSQ ratios for the averaged 2^n-frame images should be in vicinity of 2^{-n}. This is indeed the case for $n \leq 5$, so we can experimentally conclude that in our CT setup $\sigma^2 \approx \frac{256}{2^6} = 4$.

PSNR			MAE			LSQ ratio	
$u_n^{(1)}$	$v_n^{(1)}$	$u_n^{(2)}$	$u_n^{(1)}$	$v_n^{(1)}$	$u_n^{(2)}$	$u_n^{(1)}$	$u_n^{(2)}$
31.7054	38.1831	34.6291	0.0192	0.0080	0.0136	0.9970	0.4824
31.7314	37.8224	37.5529	0.0191	0.0082	0.0097	0.9881	0.2439
31.7171	38.1628	40.3758	0.0191	0.0079	0.0069	0.9900	0.1263
31.7126	38.1696	43.0911	0.0192	0.0080	0.0050	0.9923	0.0670
31.7370	38.1945	45.5668	0.0191	0.0078	0.0036	0.9854	0.0375
31.7340	38.2373	47.7526	0.0191	0.0079	0.0027	0.9895	0.0227
31.7288	37.5848	49.5081	0.0191	0.0081	0.0021	0.9787	0.0152
31.7212	38.1566	50.9980	0.0191	0.0079	0.0016	0.9919	0.0111

Table 1: Summary of the quantitative characteristics of the experiments.

An illustration that Poisson pdf is the right statistical tool for modeling noise distribution in particle-counting processes is given in Fig. 1. In the middle we plot the intensity distribution of the true image background. We see, that in practice the background is not constant, as one expects but still most of the intensities are around 235, which we take as default value. The right histogram, together with the difference image in Fig. 2 confirm the observation in [2] that our denoising method tends to oversmooth the image and that around sharp edges high-intensity pixels gave away part of their intensity to the neighboring low-intensity pixels. The maximal background intensity of $v_n^{(1)}$ is only 230, the second peek in the histogram as well as the contrasted edges in the difference image correspond to the "intensity transfer". Around the upper vertices of the cube, additional artifacts (probably due to illumination or sensor noise) appear, resulting in highly unstable intensity measuring for those two pixels (even the two 2048-frame images differ there with 10 units). Finally, the pores of the material are visible on the difference image, unlike on all the other images.

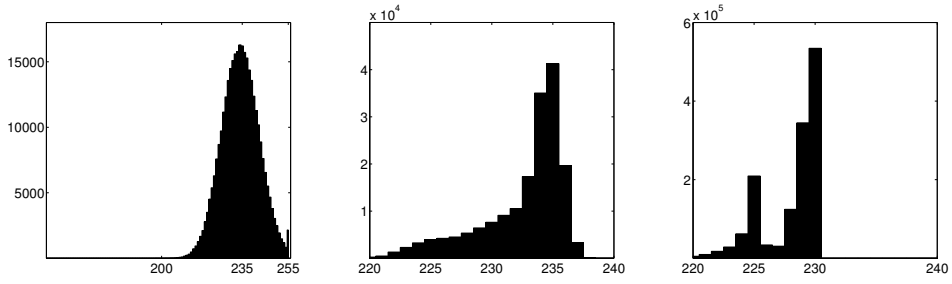

Figure 1: Histograms of: **Left:** $\cup u_n^{(1)}\big|_{u_{11}^{(2)}(i)=235}$; **Middle:** $u_{11}^{(2)}(i) > 128$; **Right:** $\cup v_n^{(1)}\big|_{u_{11}^{(2)}(i)>128}$.

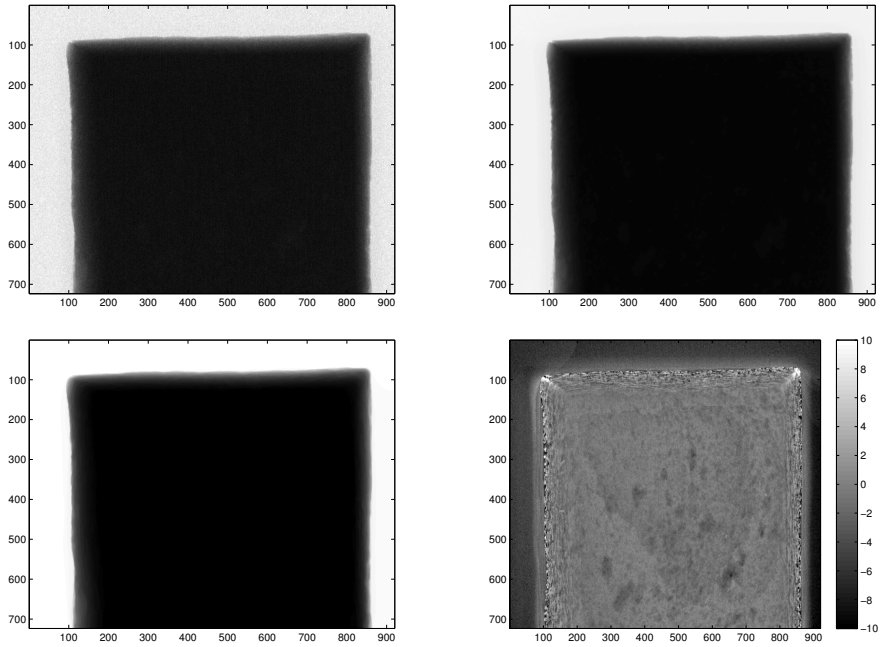

Figure 2: **Left:** Single-frame image $u_1^{(1)}$ (**top**), Denoised image $v_1^{(1)}$ (**bottom**). **Right:** 2048-frame image $u_{11}^{(2)}$ (**top**), Difference image $v_1^{(1)} - u_{11}^{(2)}$ (**bottom**).

Acknowledgement. This work was supported by the Bulgarian Academy of Sciences through the "Young Scientists" Grant No. DFNP-92/04.05.2016.

References

[1] S. Harizanov, J. C. Pesquet, and G. Steidl. Epigraphical Projection for Solving Least Squares Anscombe Transformed Constrained Optimization Problems. In *Scale-Space and Variational Methods in Computer Vision (SSVM 2013)*, A. Kuijper et al., (eds.), LNCS 7893, 125–136, Springer-Verlag: Berlin, 2013.

[2] S. Harizanov. Deblurring Poissonian Images via Multi-Constraint Optimization. In: *Innovative Approaches and Solutions in Advanced Intelligent Systems*, Studies Comp.Intelligence Vol. 648, Springer (to appear).

Metadynamics of Large Proteins with Collective Variables Preselection by a Spatiotemporal Multistage Consensus Clustering

Nevena Ilieva, Elena Lilkova, Peicho Petkov, and Leandar Litov

1 Introduction

Protein-protein interactions play a fundamental role in many biochemical processes. The development of different analytical tools for their investigation is a central problem in proteomics. Molecular dynamics (MD) [1] provides often experimentally unaccessible information for the equilibrium and transport properties of such biocomplexes that justifies the MD simulations status as *in silico* experiments. Despite the rapid increase in the computation power in last years, the attainable time range for large biosystems remains limited to microseconds on dedicated powerful supercomputers, which rises the question for the adequacy of the conformation space sampling, needed in turn for obtaining reliable macro parameters and observable quantities from the microscopic MD data.

2 Materials and Methods

Metadynamics

In many long time-scale processes involving transitions with high free energy barriers or large-scale molecular rearrangements conventional MD sampling techniques render inefficient [2], thus necessitating the development of various enhanced sampling techniques. Metadynamics [3] is such a powerful advanced technique for studying multidimensional free energy surfaces (FES) of complex systems by a non-Markovian dynamics in the collective variables (CVs) space. The key to its success is the existence of a mapping of the history-dependent dynamics into a Markovian process in the original variables, at least for evolutions of the Langevin type [4].

hIFNγ Mutated Forms

Interferon gamma (IFNγ) (Fig.1) is an important cytokine, which plays a key role in the formation and modulation of immune response (for a review, see, e.g. [5]). Its abnormal expression is associated with the etiology of many autoimmune diseases (multiple sclerosis, alopecia areata, autoimmune uveitis, myasthenia gravis, post-transplant arteriosclerosis, etc.). hIFNγ is recognized by its own species-specific receptor (hIFNγR). Introduction of stable inactive analogies of the cytokine with mutations in the residues, which do not take part in receptor recognition, but are involved

in the signaling pathway — residues from the NLS, i.e. residues Lys86-Lys-Lys88, might help blocking the hIFNγ excessive biological activity.

Spatiotemporal Multistage Consensus Clustering

The MD-data analysis is based on initial fitting procedures, aiming at separation of the global movements of the biomolecules from the relative movements and deformations of their constituents, which are relevant for the investigated molecular features, processes or mechanisms. The results of this analysis strongly depend on the fitting procedure, the reference conformation and the fitting domain. The presence therein of even small very flexible parts can contribute significantly to the RMSD values and thus compromise the fitting. For identifying of semi-rigid domains we use a multistage consensus clustering (MCC) algorithm [6], based on the variation of distances between pairs of Cα-atoms as the target function

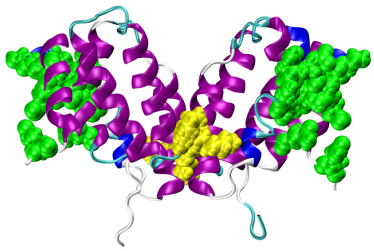

Figure 1: Secondary structure of hIFNγ, with indicated binding (green) and mutation (yellow) sites.

$$q(c) = \sum_{m=1}^{k} \sum_{i=1}^{N} \sum_{j=1}^{N} c_{im} c_{jm} S_{ij} \to \min \tag{1}$$

Here c_{im} is the claster-membership coefficient of atom i in cluser m, for N atoms and k clusters. The standard deviations of distances d_{ij} between atom pairs (i, j) along a given trajectory are contained in the STDDV matrix

$$S_{ij} = \sqrt{\frac{L}{L-1} \left\langle (d_{ij} - \langle d_{ij} \rangle)^2 \right\rangle}\,, \tag{2}$$

where L is the number of frames (conformations) considered and the average is taken over the whole or a part of the trajectory.

3 Proof-of-Concept Protocol

The reliability of metadynamics strongly depends on the choice of the CVs, which should meet a number of important criteria, in particular, the set of CVs should be able to clearly distinguish between the initial and the final state and preferably the intermediates. Ideally, the CVs should describe all the slow events that are relevant to the investigated process. The CVs must be explicit functions of the coordinates of the particles of the system and their number should be small. In most cases, finding a good

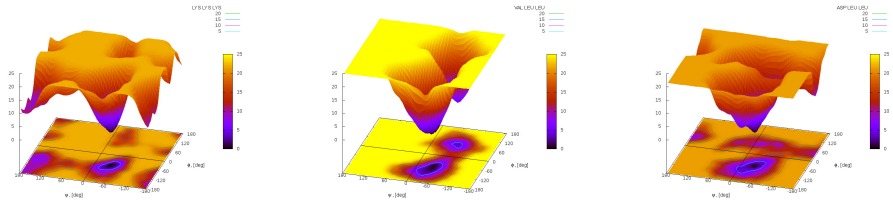

Figure 2: Free energy surface of the calibration proteins.

set of CVs is a complicated task. There is no *a priori* prescription for identification of a suitable set of CVs and the trials-and-errors remains the most common approach, which is computationally very expensive, especially for large biomolecular systems.

We aim at developing a CV selection protocol based on the rigidity of the protein conformation in the most sensitive for the investigated process domains. The structure identification is performed by means of multistage consensus clustering [2], with adequate selection of the cluster size and rigidity/flexibility parameters.

Table 1: Parameters of the calibration proteins.

Amino acid sequence in aa 86–88	Local secondary structure	RMSD [kCal/mol]	ΔG [kCal/mol]	Antiproliferative activity [IU/mg]
Lys-Lys-Lys	α-helix	0.00	16.3	5×10^7
Val-Leu-Leu	α-helix	0.12167	> 20	1.1×10^5
Asp-Leu-Leu	unfolded	0.16	> 20	none

For the selection protocol development and calibration, we have chosen three protein structures — the hIFNγ wild type and two derivative proteins out of 100 random mutations between amino aids 86-88. These were taken as representative examples for preserved, resp. destroyed structure and activity, compared to the wild type. Conclusions were based on unguided metadynamics analysis of the FES in the parameter space of Lys 86 backbone twist angles and antiproliferative activity competition bioassays [7, 8], the corresponding data being shown in Table 1. RMSD refers to the root mean square deviation between the mutant and the wild-type FES in the α-helical region of the plot and ΔG characterizes the height of the FES barrier between the α-helical and the extended-conformation regions.

[2] https://snowball1108@bitbucket.org/BioSimVienna/multistage-clustering.git

4 Discussion

Biomolecular processes having long characteristic times and involving large-scale special rearrangement of many atoms are still challenging to simulate. Advanced sampling techniques as metadynamics now allow such phenomena to be studied more efficiently, but their successful application depends strongly on the choice of the collective variables. We base our CV choise on the rigidity of the relevant for the investigated process domains of the biomolecule, identified by optimized multistage consensus clustering. In the calibration examples, this turns out to be the lowest-rigidity cluster in the binding-site domain, with an attempted CV choice (compare Fig.2) — dihedral angles of its central amino acid. The protocol will be applied in studying the hIFNγ binding to its receptos, where all intuitive CV choices are known to have failed simulating the process.

Acknowledgements

The simulations were performed on the HPC Cluster at the Faculty of Physics of Sofia University "St. Kl. Ohridski". NI and EL acknowledge financial support of the Bulgarian Academy of Sciences through the "Young Scientists" Grant No. DFNP-99/04.05.2016.

References

[1] D. Frenkel, and B. Smit, Understanding Molecular Simulation, 2nd Ed. (Academic Press, San Diego, 2002).

[2] L. Sutto, M. D'Abramo, and F.L. Gervasio, J. Chem. Theory Comput. **6** (2010) 3640-âĂŞ3646.

[3] A. Laio and M. Parrinello, Proc. Nat. Acad. Sci., **99** (2002) 12562-12566.

[4] G. Bussi, A. Laio, and M. Parrinello, Phys. Rev. Lett. **96** (2006) 090601; DOI: 10.1103/PhysRevLett.96.090601.

[5] R.G. Tsanev, I. Ivanov I. Immune Interferon: Properties and Clinical Application. (CRC Press LLC, USA, 2001), ISBN 0-8493-1148-9.

[6] M. Kenn, R. Ribarics, N. Ilieva, M. Cibena, R. Karch, W. Schreiner, Mol. BioSyst. (2016) Advance Article, DOI: 10.1039/C5MB00879D

[7] E. Lilkova, G. Nacheva, P. Petkov, P.St. Petkov, S. Markov, N. Ilieva, and L. Litov, Comp. Math. Appl. (CAMWA) **64** (2012) 272–277.

[8] G. Nacheva et al., Biotechnol. and Biotechnol. Eq. **26** (2012) 200–204. DOI: 10.5504/50YRTIMB.2011.0036 git.

Multistage Techniques for Protein Folding Disentanglement and Analysis

Nevena Ilieva, Jiaojiao Liu, Peicho Petkov, Jianfeng He, Antti Niemi

1 Introduction

The protein folding problem endures as one of the most important unresolved problems in science. Despite the Anfinsen's dogma, it is still not possible to predict the 3D structure of an arbitrary protein from its primary structure (aminoacid sequence).

We aim at developing a next generation, computationally effective precision multiscale approach to predict the structure and to model the dynamics of proteins from their amino acid sequence. To this end, we intertwine stochastic and deterministic steps, substantiated in MCMC (Markov chain Monte Carlo) and MD (molecular dynamics) approaches.

2 Combined MCMC/MD Approach

By far the most ambitious computational approach to the protein folding problem is based on classical molecular dynamics (MD) [1]. With a solid conceptual foundation in established laws of physics, MD is a very powerful method for *de novo* and even *ab initio* modeling of protein folding, able to deliver the physical evolution of the protein configurations. Due to the various energy barriers in the energy landscape the system tends to explore a vicinity of the initial-state region and might get trapped in a potential well.

Prior to MD, computer simulations of many-body systems with a very large number of accessible states were carried out within the Monte Carlo approach. The MC-based methods (e.g., the MCMC Metropolis method [2]) are stochastic in nature and rely on importance-weighted random walk in the configuration space. MC methods are not suitable for studying time-dependent phenomena or momentum-dependent properties but give better coverage through tunneling between energetically separated regions.

The approach we propose for modeling protein folding and dynamics, builds on complementarity of these two methods. We monitor the evolution of the protein geometry using Frenet frames at the positions of protein Cα atoms. In our model, the protein geometry is described in terms of virtual bond and torsion angles κ_i and τ_i, as the *complete set of structural order parameters*

$$\kappa_{i+1,i} \equiv \kappa_i = \arccos(\mathbf{t}_{i+1} \cdot \mathbf{t}_i) \tag{1}$$

$$\tau_{i+1,i} \equiv \tau_i = \mathrm{sign}[(\mathbf{b}_{i-1} \times \mathbf{b}_i) \cdot \mathbf{t}_i] \arccos(\mathbf{b}_{i+1} \cdot \mathbf{b}_i), \tag{2}$$

where $(\mathbf{t}_i, \mathbf{b}_i, \mathbf{n}_i)$ are the unit backbone tangent, binormal and normal vectors.

The modular building blocks of a folded protein can be described in terms of the kink solution of a generalized discrete non-linear Schrödinger equation (DNLS), encoding the minimum energy configuration of an effective free energy that models the thermodynamics of the protein (for details, see [3]).

$$F = \sum_{i=1}^{N} \Big\{ \lambda\,(\kappa_i^2 - m^2)^2 + \frac{q}{2}\,\kappa_i^2\tau_i^2 - p\,\tau_i + \frac{r}{2}\tau_i^2 + \dots \Big\} + \sum_{i=1}^{N-1} (\kappa_{i+1} - \kappa_i)^2 \ + \dots \quad (3)$$

Eq.(3) represents the most general Landau free energy in terms of the chosen angular variables, which is consistent with the invariance of the backbone geometry under local rotations in the $(\mathbf{n}_i, \mathbf{b}_i)$-plane. The kink is *non-perturbative* and is stable against small perturbations. Thus this concept provides an effective tool for exploration of complicated free-energy surfaces. The formation of super-secondary structures during the protein folding then can be understood in terms of a Bloch domain wall that forms along a Heisenberg spin chain, or along a closely related XY spin chain [4].

Based on these observations, we stage the folding simulation as follows:

1. A set of conformations is obtained by initial Markovian Monte Carlo time evolution with the standard, universal heat bath probability distribution [5];
2. The originating structures are clustered acording to the modular parameters;
3. Cluster representatives are subjected to all-atom MD simulations;
4. Resulting structures are investigated for stability, soliton content and certain patterns in the conformational changes;
5. If certain convergence requirements are met, the folding is completed; otherwise the whole procedure is repeated.

3 Example: Myc protein

Myc is a multifunctional nuclear phosphoprotein that can drive cell cycle progression, apoptosis and cellular transformation. Deregulation of Myc has been implicated in the development of many human cancers, including BurkittâĂŹs lymphoma, neuroblastomas, and small cell lung cancers. The structure in Protein Data Bank has a PDB ID 1NKP [6]. We shall focus on chain A, the segment Val901 – Glu979.

The energy function (3) was trained with the X-ray data for 1NKP and then subjected to heating and cooling simulations, the whole cycle encompassing 10^7 MC steps. The simulations and the structure modeling were performed with the packages *ProPro* and *CurveUI* [3]. The (κ, τ) spectrum of the X-ray structure and the comparison with the 4-kink solution are shown in Fig. 1.

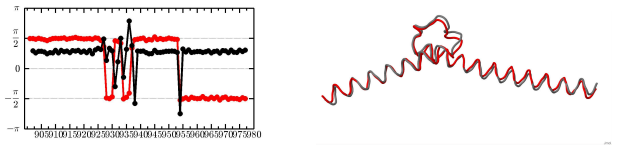

Figure 1: (a) Curvature (red) and torsion (black), of 1NKP chain A; (b) Experimental (grey) vs. modelling (red) 4-kink segment in trace representation, RMSD = 1.5628Å.

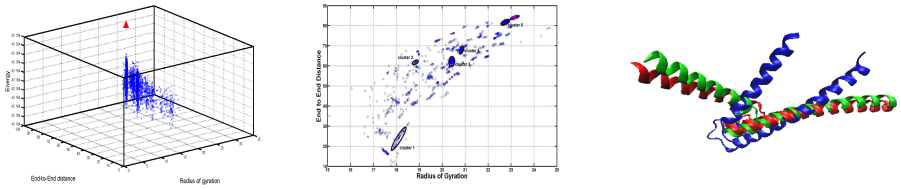

Figure 2: (a) Distribution of the final conformations in a 3D parameter space; (b) Clustering according to end-to-end distance and gyration radius; (c) Superimposition of X-ray structure (red) and the representatives of clusters [1] (blue) and [5] (green).

We selected the centroids of the biggest cluster [5] (with 161 structures) and third biggest, but furthest cluster [1] (47 structures) as initial structures for 50ns MD simulations performed with the GROMACS 4.6.3 package [7], with Gromos53a6 force field, with a time step of 2 fs. We used periodic boundary conditions at salt concentration of 0.15 mol/l and temperature 290 K, supported with Berendsen thermostat in the equilibration phase and v-rescale thermostat in the production run. The pressure was kept constant with Berendsen barostat, changed to Parrinello-Rahman in the production run, both changes aiming to ensure the generation of a proper canonical ensemble. The coordinates were recorded every 2 ps, giving rise to 2500 frames. The snapshots in Fig. 3(a) demonstrate the coherence of the three different samplings.

4 Discussion

The Myc-protein example can be considered as a proof-of-concept study for the envisaged multi-scale protocol for simualtion and analysis of the protein folding process. This protocol allows for accelerated exploration of the conformation space and faster convergence to the biological fold. We observe practical identity (within the experimental error) between the centroid of the biggest MC cluster and the experimental

[3] http://www.folding-protein.org

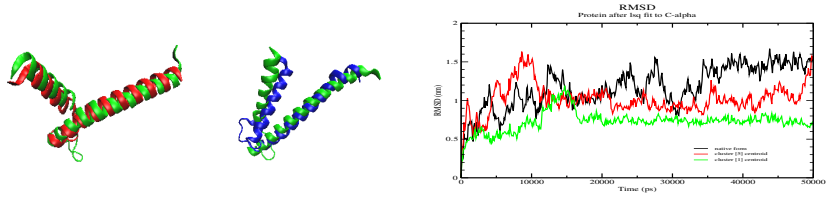

Figure 3: (a) Snapshots of shared conformatuions between PDB structure and cluster [5] in the 17.3 ns, and clusters [1] and [5] in the 7.2 ns; (b) RMSD of the Cα atoms in the selected structures along the MD trajectory.

(biological) fold. The MD evolution confirms the uniformity of the two structures. The third biggest (and furthest) cluster does not resemble the biological, however it shares evolution states with the successful fold, which shows that the two sample the same conformation space. This might be a signature for the existence of other stable or quasi-stable folds. A convergence criterion should distinguish between these two options and should also account for the exceptions from the Anfinsen dogma.

Acknowledgements

This research was supported in part by Bulgarian Science Fund (Grant DNTS-CN-01/9/2014), Qianren Grant at Beijing Institute of Technology, and Intergovernmental S&T Cooperation Project at the Ministry of Science and Technology of P.R. China.

References

[1] D. Frenkel, and B. Smit, Understanding Molecular Simulation, 2nd Ed. (Academic Press, San Diego, 2002).

[2] N. Metropolis, A.W. Rosenbluth, M.N. Rosenbluth, A.N. Teller, and E. Teller, J. Chem. Phys. **21** (1953) 1087-âĂŞ1092.

[3] A.J. Niemi, Theor. Math. Phys. **181** (2014) 1235.

[4] J. Dai, A. Niemi, J. He, A. Sieradzan, and N. Ilieva, Phys. Rev. E (2016)

[5] A. Krokhotin, M. Lundgren, A.J. Niemi, X. Peng, J. Phys. Cond. Matter **25(32)** (2013) 325103; doi: 10.1088/0953-8984/25/32/325103.

[6] S.K. Nair, S.K. Burley, Cell (Cambridge, Mass.) **112** (2003) 193âĂŞ-205.

[7] B. Hess, C. Kutzner, D. van der Spoel, E. Lindahl, J. Chem. Theory Comput. **4** (2008) 435.

Preconditioning of Flows in Heterogeneous Porous Media with High Contrast Permeability

G. Kanschat, R. Lazarov, and Y. Mao

Mathematical models of flows in porous media have been used in various industrial applications such as oil and water reservoirs, food processing, batteries, etc as well as heat and mass transfer and transport.
Such applications have motivated research in design of numerical methods and algorithms for simulation of fluid flows in highly heterogeneous porous media. At pore level, the Reynolds number is small due to the small reference length and flows of incompressible fluids can be modeled by Stokes equations. On field-scale, fluid flows in porous media have been modeled mainly by mass conservation equation and by Darcy's law $\nabla p = -\mu K^{-1}\mathbf{u}$ between the macroscopic pressure p and velocity $\mathbf{u}$, which we write down on the form $\nabla p = -\kappa(x)\mathbf{u}$. Here $K(x)$ is the media permeability and μ is the fluid viscosity.

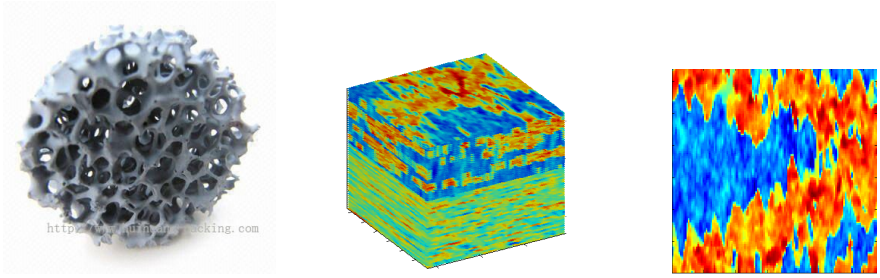

Figure 1: Left: CT scans of industrial foam on a micro-scale; Center: computer generated 3-D permeability of benchmark SPE10; Right: slice 44 of of SPE10 [7]

Many porous media are characterized by very low solid volume fraction (or high porosity), e.g. fractured or vuggy reservoirs, mineral wool, and industrial foams, (cf. Figure 1: Left). For such media the porosity could be as high as 95 – 98 %. For such highly porous media and Darcy's law often does not give good agreement with the experimental data. In order to reduce the deviations between the measurements for flows in highly porous media and the Darcy-based predictions, Brinkman in [2] introduced a new phenomenological relation between the fluid velocity $\mathbf{u}$ and the pressure gradient: $\nabla p = -\kappa(x)\mathbf{u} + \mu\Delta\mathbf{u}$. Together with conservation of mass, which in the absence of any mass sources or sinks is expressed by $\nabla \cdot \mathbf{u} = 0$, Brinkman equations and proper boundary conditions form a closed mathematical model.
An important characteristic is the contrast of the media $\boldsymbol{\kappa}$, defined as the ratio between the highest and lowest values of the permeability, $\boldsymbol{\kappa} = \max_{x\in\Omega} K(x)/\min_{x\in\Omega} K(x)$.
The problems we consider in this paper involve $K(x)$ that varies substantially on a small scale, corresponding to high frequency and high contrast media.

Design and testing of multiscale numerical methods for Darcy and Brinkman equations was done, for example, in [3, 6] and [5], respectively. These methods could be used either (1) as a stand-alone numerical upscaling procedure that involves fine and coarse grids or (2) as robust (with respect to the high contrast media properties) iterative solvers for the finite element approximation on a very fine mesh. The robustness of the upscaling method is achieved via special construction of a coarse grid space that includes patched together eigenfunctions corresponding to the smallest eigenvalues of properly weighted local spectral problems [4, 5]. Such approximation and solution methods are based on some recent advances in discontinuous Galerkin finite element methods (e.g. [3, 5]) and multiscale finite element method (e.g. [6]) and the solution strategies for solving the corresponding algebraic systems, [4, 5, 12].

Here we present a unified approach for approximation and solving the Brinkman/Darcy flow equations by H^{div}-conforming Raviart-Thomas mixed finite elements. The discretization is done on fine meshes resolving meso-scale heterogeneity of the media. For example, in our computations certain media are discretized on a mesh with 256^d or 512^d ($d = 2, 3$ is the space dimension) cells/voxels. Discretization on such grid results in a very large algebraic saddle point problem which is ill-conditioned due to both, the small mesh-size and high contrast $\boldsymbol{\kappa}$. The numerical simulation of processes in media of high frequency and high contrast represent a great challenge for the computational practice. In our opinion, its efficient preconditioning is not fully mastered yet. In the talk we present a step in this direction, namely, multi-grid preconditioner of Brinkman/Darcy system that uses a smoother based on overlapping domain decomposition technique (e.g. [8, 11]). It is based on the work of Arnold, Falk, and Winther, [1] for preconditioning systems involving H^{div}-norm.

The proposed preconditioner is based on a monolithic multi-grid framework that operates on the saddle point system directly. This differs from the block diagonal preconditioner developed in [10] for Darcy model. We have compared the performance of these two methods on permeability field generated by slice 44 of SPE10 benchmark, see Figure 1 (Right). The total number of iterations in the minimal residual method in [10] is slightly less than the iterations of our method. However, within each iteration the method, to invert the block corresponding to the weighted H^{div}-norm, the method in [10, Tables 12 and 13] uses in average 6 inner multilevel iterations. Nevertheless, the computational complexity of both methods is similar and experimentally they both show robustness with respect to the high contrast in the case of Darcy flows.

In the talk we shall also discuss:

(1) A unified solution methodology for computer simulation of flows in porous media modeled by Darcy and Brinkman equations. Using this methodology, one may set up natural experiments with highly heterogeneous media in order to compare and analyze the numerical simulations in the framework of a mathematical modeling tool.

(2) Experimental testimony of the efficiency of the developed preconditioner for solving very large systems of linear equations arising from the finite element approximation of the Darcy and Brinkman equations and demonstration (via various tests) of robustness with respect to both, the mesh step-size and the high contrast high frequency porous media. Our numerics shows that the proposed preconditioner is efficient and

robust with respect to the contrast in Brinkman flows. However, we see increase of the number of iterations when the contrast grows, e.g. for growth of contrast from 10^4 to 10^6 the number of GMRES iterations increases 2.5 times.
(3) Various two- and three-dimensional numerical test problems that are used by flow in porous media community in order to demonstrate the capabilities of numerical simulation methodology for relevant applications. As a modeling tool, these numerical experiments also show the difference in the flow intensity (pressure and velocity) produced by Darcy and Brinkman mathematical models. As seen from Figure 2, the flow patterns are quite similar but the velocity fields obtained by Darcy and Brinkman models differ significantly.

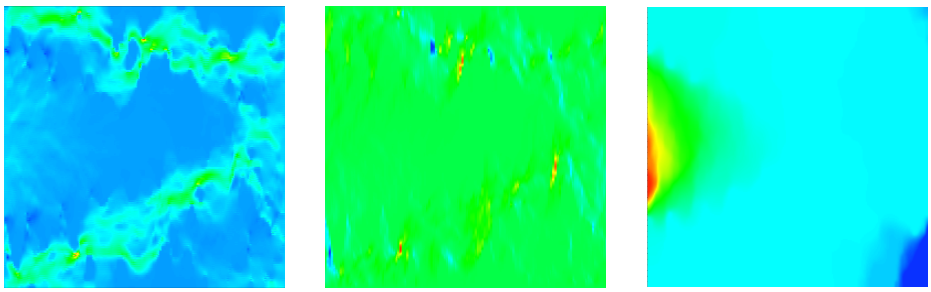

(a) Darcy: u_1 (b) Darcy: u_2 (c) Darcy: p

(d) Brinkman: u_1 (e) Brinkman: u_2 (f) Brinkman: p

Figure 2: Solutions of 2-D Darcy (first row) and Brinkman (second row) models for permeability data of slice 44 in the same color scale

References

[1] D. Arnold, R. Falk, and R. Winther, Preconditioning in H(div) and Applications, *Math. Comput.*, 66 (1997) 957–984

[2] H. Brinkman, A Calculation of the Viscous Force Exerted by a Flowing Fluid on a Dense Swarm of Particles, *Appl. Sci. Res.*, A1 (1947) 27–34

[3] Y. Efendiev, R. Lazarov, and K. Shi, A Multiscale HDG Method for Second Order Elliptic Equations. Part I. Polynomial and Homogenization-based Multiscale Spaces, *SIAM J. Numer. Anal.*, 53(1) (2015) 324–369

[4] Y. Efendiev, and J. Galvis, Domain Decomposition Preconditioners for Multiscale Flows in High Contrast Media, *Multiscale Modeling and Simulation*, 8(4) (2010) 1461–1483

[5] Y. Efendiev, J. Galvis, R. Lazarov, and J. Willems, Robust Domain Decomposition Preconditioners for Abstract Symmetric Positive Definite Bilinear Forms, *ASAIM: Mathematical Modeling and Numerical Analysis*, 46 (2012) 1175–1199

[6] Y. Efendiev and T. Hou, *Multiscale FEM. Theory and Applications*, Springer, 2009

[7] S. P. E. International, SPE10 Comparative Solution Project: general information and description of model 2, 2000, http://www.spe.org/web/csp/#datasets

[8] G. Kanschat and Y. Mao, Multigrid Methods for H(div)-conforming Discontinuous Galerkin for the Stokes Equations, *J. Numer. Math.*, 23(1) (2015) 51–66

[9] G. Kanschat, R. Lazarov, and Y. Mao, Geometric MG for Darcy and Brinkman Models of Flows in Highly Heterogeneous Porous Media: A Numerical Study, *J. Comput. Appl. Math.*, (submitted, 2016), arXiv:1602.04858

[10] J. Kraus, R. Lazarov, M. Lymbery, S. Margenov, and L. Zikatanov, Preconditioning heterogeneous H(div) problems by additive Schur complement approximation and applications, *accepted in SIAM J. Sci. Comput.* (posted as arXiv:1406.4455)

[11] Y. Mao, *Geometric Multigrid Methods for Flow Problems in Highly Heterogeneous Porous Media*, PhD thesis, Texas A&M University, College Station, 2014

[12] J. Willems, Robust Multilevel Methods for General Symmetric Positive Definite Operators, *SIAM J. Numer. Anal.*, 52(1) (2014) 103–124

Numerical penalization algorithms for pricing American options

Miglena N. Koleva, Radoslav L. Valkov

The pricing of early-exercise securities is important in quantative finance because these are the most widely-traded type of instruments on the derivative market. The American-style option valuation is an illustrative example of an optimal stopping time problem which could be further formulated as a parabolic variational inequality.
Let S stand for the underlying asset price process, following a standard geometric Brownian motion with volatility σ and drift equal to the interest rate r while t is the time to maturity. For computational purposes one must truncate the spatial domain $S \in [0, \infty)$ and introduce the far field boundary location $S_{\max}$. For clarity we consider pricing a put with strike K and the following conditions on the parabolic boundary:

$$V(S,0) = V^*(S) := \max(K - S, 0), \quad V(0,t) = K, \quad V(S_{\max}, t) = 0.$$

A rule of the thumb says "$S_{\max}$ is a few times the strike price K". The American put is a classical Stefan problem where the payoff is convex, continuous but nonsmooth. The option value with maturity T satisfies the parabolic variational inequality

$$LV(S,t) := V_t - \frac{1}{2}\sigma^2 S^2 V_{SS} - rV_S + rV \geq 0 \perp V(S,t) \geq V^*(S) \ \text{ a.e. in } \ (0,\infty)\times[0,T)$$

which could be written down as the following linear complementarity problem (LCP)

$$\begin{cases} LV(S,t) = \lambda \geq 0, \\ V(S,t) - V^*(S) \geq 0, \quad LV(S,t) \cdot (V(S,t) - V^*(S)) = 0 \end{cases}$$

From the complementarity condition

$$V \geq V^*, \ \lambda \geq 0, \ \lambda \cdot (V(S,t) - V^*(S)) = 0$$

we infer for the Lagrange multiplier

$$\lambda = \max\left(0, \lambda + \epsilon^{-1}(V^* - V)\right)$$

for any sufficiently small (penalty) parameter $\epsilon > 0$. Thus, we get to solve the following nonlinear equation, equipped with the complementarity condition and drawing analogies with the augmented Lagrangian method:

$$LV(S,t) - \max\left(0, \lambda + \epsilon^{-1}(V^* - V)\right) = 0.$$

Superimposing infinite penalty when violating the constraint $V(S,t) - V^*(S) \geq 0$ we may embed the LCP in the family of the nonlinear equations

$$LV_\epsilon(S,t) - \max\left(0, \epsilon^{-1}(V^* - V_\epsilon)\right) = 0. \tag{1}$$

The penalty method guarantees in an asymptotic sense the fulfilment of constraints by including in the objective function an additional penalty term. If we consider the upper bound on the multiplier $\Lambda_{\max}$ we may state the following approximation, see [1]:

$$LV_\epsilon(S,t) - \max\left(0, \Lambda_{\max} + \epsilon^{-1}(V^* - V_\epsilon)\right) = 0. \tag{2}$$

There are, however, some issues with this approach since the early exercise constraint is not strictly satisfied by the solution for fixed small ϵ while the penalty term is nonsmooth and unbounded. The following interior approximation aims to tackle these drawbacks with $\mathrm{C} \geq rK$ for pricing the American put, cf. [2],

$$LV_\epsilon(S,t) - \frac{\epsilon \mathrm{C}}{V_\epsilon + \epsilon - (K - S)} = 0 \tag{3}$$

where the general interior penalty method, applicable to any type of payoff, is

$$LV_\epsilon(S,t) - \frac{\epsilon \mathrm{C}}{V_\epsilon + \epsilon - V^*} = 0. \tag{4}$$

[4] prove convergence of the penalized solution V_ϵ to the solution of the underlying variational inequality V. However, a major issue with this approach is its dependence on ϵ and some vague parameter C, resulting in overall lower accuracy and more Newton iterations per time level.

We therefore consider modifying this interior barrier method in order to enhance the performance. Let us set up the fully-discrete LCP in order to present our considerations in a clear and concise manner. First, by the method of lines, we define a smooth nonuniform spatial grid and approximate the spatial derivatives by second-order finite difference formulas. After backward Euler time discretization with step Δt we have to solve the following discrete linear complementarity problem for $U_n \in \mathbb{R}^{m-1}$

$$\begin{cases} (I - \Delta t A)U_n = U_{n-1} + \Delta t g + \Delta t \lambda_n \\ \lambda_n \geq 0, \quad U_n \geq U_0, \quad \lambda_n \cdot (U_n - U_0) = 0, \end{cases}$$

where $A \in \mathbb{R}^{(m-1)\times(m-1)}$ stands for the spatial discretization matrix, $g \in \mathbb{R}^{m-1}$ is the boundary information (assuming Dirichlet conditions on the elliptic boundary) and $\lambda_n \in \mathbb{R}^{m-1}$ is the nonnegative auxiliary (multiplier) vector which satisfies

$$\lambda_n = \max\left(0, \lambda_n + \frac{1}{\Delta t}(U_0 - U_n)\right).$$

The solution U_n of the discrete LCP is the saddle point of the Lagrange functional

$$\Lambda(U_n, \lambda_n) = \frac{1}{2}(I - \Delta t A)U_n \cdot U_n - b_n \cdot U_n - \Delta t \lambda_n \cdot (U_n - U_0), \ b_n := U_{n-1} + \Delta t g.$$

Let us now observe the following equivalence [3]

$$U_n - U_0 \geq 0 \Leftrightarrow \varepsilon \log\left(1 + \varepsilon^{-1}(U_n - U_0)\right) \geq 0$$

Figure 1: Put Option Value and Free Boundary

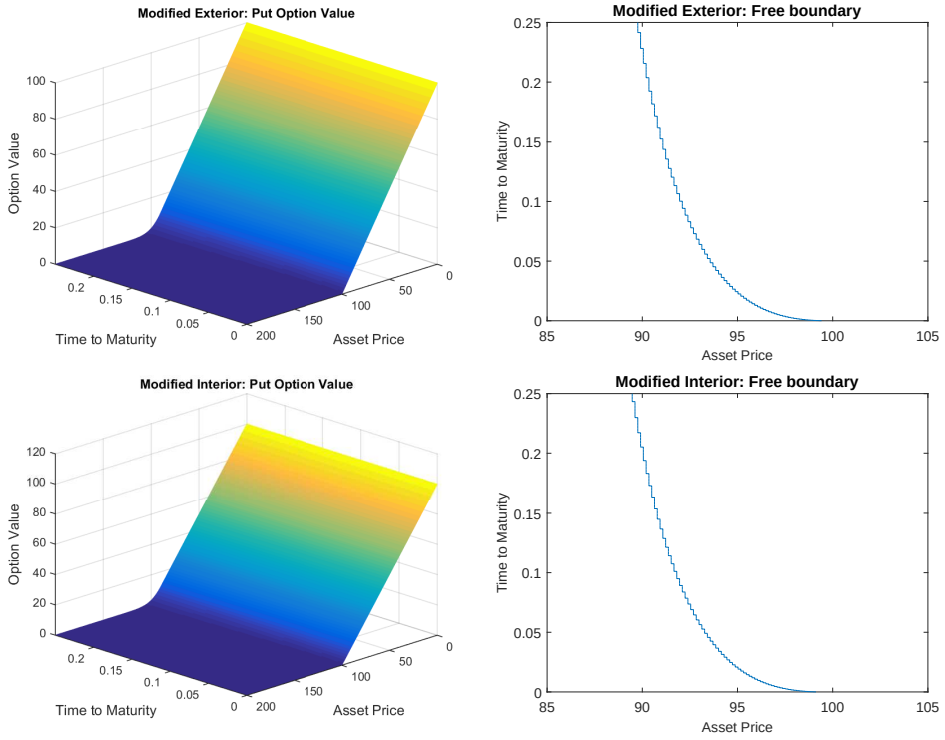

and further we shall modify the Lagrange functional accordingly

$$\Lambda(U_n, \lambda_n) = \frac{1}{2}(I - \Delta t A)U_n \cdot U_n - b_n \cdot U_n - \Delta t \lambda_n \cdot (\varepsilon \log\left(1 + \varepsilon^{-1}(U_n - U_0)\right)).$$

After applying the Karush-Kuhn-Tucker conditions we get the following discrete LCP:

$$\begin{cases} (I - \Delta t A)U_n - \Delta t \lambda_n \frac{\varepsilon}{U_n - U_0 + \varepsilon} = b_n \\ \lambda_n \geq 0, \quad U_n \geq U_0, \quad \lambda_n \cdot (U_n - U_0) = 0. \end{cases} \tag{5}$$

As a matter of fact, if we consider the fairly rough estimate for the multiplier $\lambda_n \leq rK$ in the put case we get the discrete interior penalty method Eq. (4):

$$(I - \Delta t A)U_n - \Delta t \frac{rK\varepsilon}{U_n - U_0 + \varepsilon} = b_n.$$

Substituting $U_0 = \max(K - S, 0)$ with $K - S$ as in Eq. (3) is a band-aid for the case of put option to fix the accuracy and minimize the penalty term in the continuation region where $S > K$, far away from the free boundary.

This paper is focused on comparing numerically the known penalty methods and the newly proposed modified barrier approach. We present numerical algorithms for the modified exterior and interior methods with the aim to investigate their properties in detail. These perform well, showing reliable and efficient results on Figure 1.

Acknowledgements: This research was supported by the European Union under Grant Agreement number 304617 (FP7 Marie Curie Action Project Multi-ITN STRIKE - Novel Methods in Computational Finance, the Bulgarian National Fund of Science under Project I02/20-2014 and partly by 2016-FNSE-03.

References

[1] K. Ito, L. Kunish, Parabolic variational inequalities: the Lagrange multiplier approach, J. Math. Pures. Appl. 85 (2006) pp. 415-449.

[2] B.F. Nielsen, O. Skavhaug, A. Tveito, Penalty and front-fixing methods for the numerical solution of American option problems, J. Comp. Finance 5(4) (2001) pp. 69-97.

[3] R.A. Polyak, Modified barrier functions (theory and methods), Math. Programming 54 (1992) pp. 177-222.

[4] K. Zhang, S. Wang, Convergence property of an interior penalty approach to pricing American option, J. Industr. Managem. Optim. 7 (2011) pp. 435-447.

Optimal System of Strengthening Ties for the Seismic Upgrading of RC Structures Environmentally Degradated: A Computational Approach

Angelos Liolios, Konstantinos Liolios, Krassimir Georgiev, and Ivan Georgiev

In Civil Engineering, non-usual extremal actions (seismic, environmental etc.) can cause significant strength degradation and damages on existing reinforced concrete (RC) structures. To overcome such strength degradation effects, various repairing and strengthening procedures can be used for the seismic upgrading of existing RC buildings [1, 2, 3]. Among them, cable-like members (ties) can be used as a first strengthening and repairing procedure [4]. These cable-members can undertake tension, but buckle and become slack and structurally ineffective when subjected to a sufficient compressive force. So, in the mathematical problem formulation, the constitutive relations for cable-members include also inequality conditions. Such inequality conditions govern also the piece-wise linearized constitutive relations describing the non-linear behavior of the usual RC structural elements. Due to above considerations, the full problem of the earthquake response of RC structures strengthened by cable-elements bracings has as governing conditions both, equalities as well as inequalities. Thus the problem becomes a high nonlinear one. For the strict mathematical treatment of the problem, the concept of variational and/or hemivariational inequalities can be used and has been successfully applied [5]. As concerns the numerical treatment, non-convex optimization algorithms are generally required cite[6, 7]. The present study deals with two numerical approaches for the earthquake analysis of existing reinforced concrete (RC) building frames, which after their seismic assessment have to be strengthened by cable elements. The unilateral behaviours of the cable-elements and the non-linear behavior of the RC elements, are taken strictly into account and result to inequality constitutive conditions. The finite element method is used for space discretization in combination with a time discretization scheme. First, the RC frame structural system is discretized in space by using finite elements. The usual frame elements are used for the reinforced concrete frame. On the other hand, for the cable strengthening system, pin-jointed bar elements are used. The behaviour of both, the cable elements and the non-linear RC elements, includes loosening, elastoplastic or/and elastoplastic-softening-fracturing and unloading - reloading effects. All these characteristics can be expressed mathematically by non-convex relations of the general form:

$$s_i(d_i) \in \hat{\partial} S_i(d_i) \tag{1}$$

Here s_i and d_i are generalized stress and deformation quantities, respectively, $\hat{\partial}$ is the generalized gradient and S_i is the superpotential function, see Panagiotopoulos [5]. In specializing details, for the cables, s_i is the tensile force (in [kN]) and d_i the deformation (elongation) (in [m]), of the i-th cable element.

By definition -see [5] - the relation (1) is equivalent to the following hemivariational inequality, expressing the Virtual Work Principle:

$$S_i^{\uparrow}(d_i, e_i - d_i) \geq s_i(d_i) \cdot (e_i - d_i), \tag{2}$$

where $S_i^{\uparrow}$ denotes the subderivative of S_i and e_i, d_i are kinematically admissible (virtual) deformations.
Next, the dynamic equilibrium for the structural system, considered as unstrengthened, i.e. without cables, is expressed by the usual matrix relations of Structural Dynamics:

$$\mathbf{M\ddot{u}} + \mathbf{C}(\dot{\mathbf{u}}) + \mathbf{K}(\mathbf{u}) = \mathbf{f} \tag{3}$$

Here $\mathbf{u}$ and $\mathbf{f}$ are the displacement and the loading forces time dependent vectors, respectively. The damping and stiffness terms, $\mathbf{C}(\dot{\mathbf{u}})$ and $\mathbf{K}(\mathbf{u})$, respectively, concern the general non-linear case. Dots over symbols denote derivatives with respect to time. For the case of ground seismic excitation $\mathbf{x_g}$, the loading history term $\mathbf{f}$ becomes

$$\mathbf{f} = -\mathbf{M r \ddot{x}_g} \tag{4}$$

where $\mathbf{r}$ is the vector of stereostatic displacements. When cable-elements and pounding are taken into account, equations (3) for the assembled system considered as strengthened, becomes

$$\mathbf{M\ddot{u}} + \mathbf{C}(\dot{\mathbf{u}}) + \mathbf{K}(\mathbf{u}) = \mathbf{f} + \mathbf{Ts} \tag{5}$$

Here $\mathbf{s}$ is the cable elements stress vector and $\mathbf{T}$ is a transformation matrix.
The system of the above relations (1)–(5), combined with the initial conditions, provide the problem formulation, where, for given $\mathbf{f}$ and/or $\ddot{\mathbf{x}}_\mathbf{g}$, the vectors $\mathbf{u}$ and $\mathbf{s}$ have to be computed.
The relevant computational approach is described in [3, 4]. A piecewise linearization of the above constitutive relations as in elastoplasticity is used(see e.g. Fig. 1.B). By applying a time-integration scheme, in each time-step Δt a relevant non-convex linear complementarity problem of the following matrix form is eventually solved :

$$\mathbf{v} \geq \mathbf{0}, \quad \mathbf{Av} + \mathbf{a} \leq \mathbf{0}, \quad \mathbf{v^T} \cdot (\mathbf{Av} + \mathbf{a}) = \mathbf{0}. \tag{6}$$

Here $\mathbf{v}$ is the vector of unknown unilateral quantities at the time âĂŞmoment t, $\mathbf{v^T}$ is the transpose of $\mathbf{v}$, $\mathbf{a}$ is a known vector dependent on excitation and results from previous time moments $(t - \Delta t)$, and $\mathbf{A}$ is a transformation matrix.
An alternative approach for treating numerically the problem is the incremental one. Now, relations (5), taking into account also second-order geometric effects (P-Delta effects), are written in incremental form:

$$\mathbf{M\Delta\ddot{u}} + \mathbf{C\Delta\dot{u}} + (\mathbf{K} + \mathbf{G})\mathbf{\Delta U} = -\mathbf{M\Delta\ddot{u}_g} + \mathbf{T\Delta s} \tag{7}$$

Here $\mathbf{G}$ is the geometric stiffness matrix, by which P-Delta effects are taken into account.
On such incremental approaches is based the structural analysis software Ruaumoko [8]. Ruaumoko software uses the finite element method and permits an extensive

parametric study on the inelastic response of structures. Concerning the time-discretization, implicit or explicit approaches can be used. Here the Newmark implicit scheme is chosen and Ruaumoko is used to provide results which are related to the following critical parameters: local or global structural damage, maximum displacements, interstorey drift ratios, development of plastic hinges.

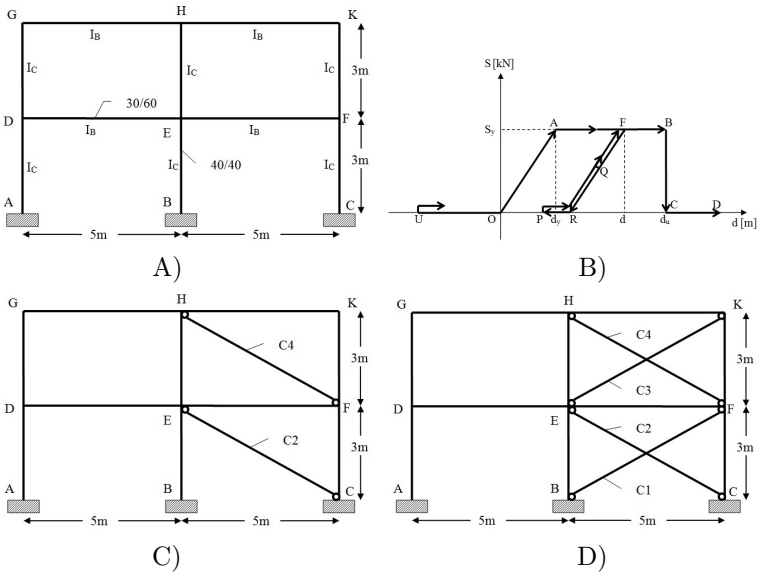

Figure 1: Numerical example: A) The two-bays two-storey RC frame; B) The constitutive law of cable-elements; C) The F2 ties-system; D) The F4 ties-system.

The decision about a possible strengthening for an existing structural system, damaged by a seismic or environmental event, can be taken after an assessment realization [2, 3]. Here the assessment is based on a relevant evaluation of suitable damage indices. After Park/Ang [10], the global damage is obtained as a weighted average of the local damage at the section ends of each structural element or at each cable element. First the local damage index DI_L is computed by the following relation:

$$DI_L = \frac{\mu_m}{\mu_u} + \frac{\beta}{F_y d_u} E_T \tag{8}$$

where: μ_m is the maximum ductility attained during the load history, μ_u the ultimate ductility capacity of the section or element, β a strength degrading parameter, F_y the yield generalized force of the section or element, E_T the dissipated hysteretic energy, and d_u the ultimate generalized deformation. As known [2, 3], ductility concerns the metelastic behaviour, see e.g. Fig. 1.B, and in terms of a generalized deformation d is defined by the relation $\mu = d/d_y$, where d_y denotes the yield generalized deformation and it holds $d \geq d_y$.

Next, the dissipated energy $\mathbf{E_T}$ is chosen as the weighting function and the global damage index $\mathbf{DI_G}$ is computed by using the following relation:

$$DI_G = \frac{\sum_{i=1}^{n} DI_{Li} E_i}{\sum_{i=1}^{n} E_i} \tag{9}$$

where: DI_{Li} is the local damage index after Park/Ang at location i, E_i is the energy dissipated at location i and n is the number of locations at which the local damage is computed.
Finally, for the choice of the optimal system of the strengthening ties, various virtual such systems are proposed and the minimum value according to (9) is sought, that is the problem $DI_G \rightarrow min$ has to be solved.
The applicability of the proposed method for selecting the optimal ties system is verified in numerical examples, e.g. as shown in Fig. 1. The RC frame to be upgraded under multiple earthquakes is shown in Fig. 1.A. The constitutive law of cable-elements is shown in Fig. 1.B. The two proposed ties strengthening systems are shown in Fig. 1.C and Fig. 1.D. The numerical results prove that the optimal system is that one of Fig. 1.D. Further details, concerning the seismic response of cable-braced RC systems subjected to multiple earthquakes, are described in [9].

References

[1] Bertero V. V., Whittaker A. S., Seismic upgrading of existing buildings, *5as Jornadas Chilenas de SismologÃηa e IngenierÃηa AntisÃησmica*, 1 (1989), 27-46.

[2] Penelis Ge., Penelis Gr., Concrete Buildings in Seismic Regions. CRC Press., (2014)

[3] Fardis, M. N., Seismic design, assessment and retrofitting of concrete buildings: based on EN-Eurocode 8 , Springer, (2009)

[4] Markogiannaki O., Tegos I., Strengthening of a Multistory R/C Building under Lateral Loading by Utilizing Ties. Applied Mechanics and Materials, 82, 559-564, (2011)

[5] Panagiotopoulos P.D., Hemivariational Inequalities. Applications in Mechanics and Engineering, Springer-Verlag, Berlin, New York, (1993).

[6] Liolios A., A linear complementarity approach for the non-convex seismic frictional interaction between adjacent structures under instabilizing effects, Journal of Global Optimization, 17 (2000), 259-266.

[7] Liolios Ang., Chalioris K., Liolios Ast., Radev St., and Liolios Kon., A Computational Approach for the Earthquake Response of Cable-braced Reinforced Concrete Structures under Environmental Actions, LNCS, 7116 (2012), 590-597.

[8] Carr A.J., RUAUMOKO - Inelastic Dynamic Analysis Program, Department of Civil Engineering, University of Canterbury, Christchurch, New Zealand, 2008.

[9] Liolios Ang., Liolios Ast., Hatzigeorgiou G., A Numerical Approach for Estimating the Effects of Multiple Earthquakes to Seismic Response of Structures Strengthened by Cable-Elements, Journal of Theoretical and Applied Mechanics, 43(3) (2013), 21-32.

[10] Park Y.J., A.H.S. Ang, Mechanistic seismic damage model for reinforced concrete, Journal of Structural Division ASCE, 111(4), (1985), 722âĂŞ739.

Selection of the Optimal Adsorption Model Concerning TP Removal in Horizontal Subsurface Flow Constructed Wetlands: A Computational Investigation

Konstantinos Liolios, Vassilios Tsihrintzis
Krassimir Georgiev, and Ivan Georgiev

1 Introduction

The use of Horizontal Subsurface Flow Constructed Wetlands (HSF CW) for wastewater treatment is recently a popular ecological and ecological solution, see f.e. [1, 2, 3, 4, 5]. The investigation of the ability of these systems to remove pollutants is a very interesting parameter for the optimal construction and operation of HSF CW [6, 7, 8]. In the essential municipal pollutants is included the Total Phosphorus (TP), for which the phenomenon of adsorption is a governing one.
In the present study, a numerical simulation concerning TP removal in HSF CW is presented. The selection of the optimal adsorption model is obtained, by using inverse problems procedures [9]. In the relevant computational investigation, a comparison between the Freundlich linear and the Langmuir non-linear isotherms for the adsorption, on the basis of available experimental data, is realized. The used experimental data are from five pilot-scale HSF CW as described in details in [4, 10]. The Visual MODFLOW computer code family [11, 12], based on the finite difference method (FDM), was used for the numerical simulations. Concerning the linear case of the Freundlich isotherm, some results have already been presented in [13].

2 The mathematical formulation of the problem

The partial differential equation (PDE), which describes in the three-dimensional (3-D) space the advection, dispersion, and removal of a solute considering sources/sinks, equilibrated adsorption and first-order irreversible kinetic reactions, is in tensorial notation $(i, j = 1, 2, 3)$ [14]:

$$\theta R_d \frac{\partial C}{\partial t} = \frac{\partial}{\partial x_i}\left(\theta D_{ij} \frac{\partial C}{\partial x_j}\right) - \frac{\partial}{\partial x_i}\left(q_i C\right) + q_s C_s - \lambda_1 \theta C - \lambda_2 \rho_b S \qquad (1)$$

where θ is the porosity, in [%]; C the aqueous solute concentration, in $[ML^{-3}]$; D_{ij} the hydrodynamic dispersion coefficient tensor, in $[L^2T^{-1}]$; C_s the concentration of the source or sink flux, in $[ML^{-3}]$; q_s the volumetric flow rate per unit volume of aquifer, representing fluid sources (positive) or sinks (negative), in $[T^{-1}]$; q_i the Darcy velocity, in $[LT^{-1}]$; ρ_b the dry bulk density of the soil, in $[ML^{-3}]$; S the concentration

adsorbed by the solid phase of the porous medium, in [M pollutant/M solid]; and λ_1 and λ_2 are the removal coefficients for the dissolved and adsorbed phases respectively, both in [T^{-1}]. Here, as usually in environmental engineering praxis, it is assumed: $\lambda_1 = \lambda_2 = \lambda$.
In Equation (1), R_d is the retardation factor [dimensionless], which is given by the equation:

$$R_d = 1 + \frac{\rho_b}{\theta} \frac{\partial S}{\partial C} \tag{2}$$

Regarding the dependence of S on C, i.e. $S = f(C)$, the most frequently used sorption isotherms are the Freundlich and Langmuir ones [14].
The linear Freundlich isotherm is expressed by the Equation:

$$S = K_d \cdot C \tag{3}$$

where K_d is the distribution coefficient, in [$L^3 M^{-1}$], which expresses the distribution of the pollutant concentrations between solid and liquid phases, S and C, respectively,.
The non-linear Langmuir isotherm is described by the equation:

$$S = S_{max} \frac{K_L C}{1 + K_L C} \tag{4}$$

where S_max is the maximum adsorption capacity in [M pollutant / M solid]; and K_L the Langmuir constant, in [$L^3 M^{-1}$].
The above equations (1), (2) and (3) or (4), combined with the groundwater flow equation and the Darcy velocity relationship [14], formulate a system of PDE equations. The solution of this system, under appropriate boundary and initial conditions, provides the five main space-time functions of the hydraulic head h, the Darcy velocities field q_i (where $i = 1, 2, 3$) and the solute concentration C.
The aim of the present study is to investigate which of the two adsorption models, the linear Freundlich isotherm of equation (3) or the non-linear Langmuir isotherm of equation (4), approaches better the experimental operation of the pilot-scale HSF CW, described in [4, 10].

3 Representative results and conclusions

The main unknown parameters of the adsorption problem are: λ, K_d, S_{max} and K_L. Concerning the distribution coefficient K_d, the oprimal value of $0.1 cm^3/g$ has been chosen, according to the type of porous media of the pilot-scale HSF CW, the inflowing concentration of TP and literature values. The values of the first-order removal coefficient λ were determined by using a trial-and-error procedure. For more details, see [13]. The values for the Langmuir constant KL and for the maximum adsorption capacity Smax were determined by using the least square methods. The results show that the linear Freundlich isotherm describes slightly better the operation for the pilot-scale HSF CW units, described in [4, 10], comparing with the non-linear Langmuir isotherm. The proposed values of the parameters λ, K_d, S_{max} and K_L can

be used effectively for the optimum design of HSF CW, both pilot-scale or full-scale, and for their construction and operation with an ecological and economical way.

Acknowledgement

This work was supported by the Bulgarian Academy of Sciences through the "Young Scientists" Grant No. DFNP-97/04.05.2016.

References

[1] Kadlec, R.H., Wallace, S., Treatment Wetlands. 2nd Edition, CRC Press, Boca Raton, FL, USA (2009)

[2] Vymazal, J., Kröpfelová, L., Wastewater Treatment in Constructed Wetlands with Horizontal Sub-surface Flow. Springer, Berlin (2008)

[3] Gikas, G.D., Tsihrintzis, V.A. On-site Treatment of Domestic Wastewater Using a Small-Scale Horizontal Subsurface Flow Constructed Wetland. Water Science and Technology J. 62(3), 603-614 (2010)

[4] Akratos, C.S., Tsihrintzis, V.A., Effect of Temperature, HRT, Vegetation and Porous Media on Removal Efficiency of Pilot-scale Horizontal Subsurface Flow Constructed Wetlands. Ecological Engineering J. 29, 173-191 (2007)

[5] Vera, I., Garcia, J., Saez, K., Moragas, L., Vidal, G., Performance Evaluation of Eight Years Experience of Constructed Wetland System in Catalonia as Alternative for Small Settlements. Ecological Engineering J. 37(2), 364-371 (2011

[6] Vymazal, J., Removal of Phosphorus in Constructed Wetlands with Horizontal Sub-Surface Flow in the Czech Republic. Water, Air and Soil Pollution: Focus J., 657-670 (2004)

[7] Drizo, A, Frost, A.C., Grace, J., Smith, A.K., Physico-Chemical Screening of Phosphate-Removing Substrates for Use in Constructed Wetland Systems. Water Research J. 33 (17), 3595âĂŞ3602 (1999)

[8] Brix, H., Arias, C.A., Del Bubba, M., Media Selection for Sustainable Phosphorus Removal in Subsurface Flow Constructed Wetlands, Wat. Sci. and Techn. J. 44(11-12). 47-54 (2001)

[9] Sun, N.Z., Inverse Problems in Groundwater Modeling, Springer Science and Business Media, Berlin (2013)

[10] Liolios, K.A., Moutsopoulos, K.N., Tsihrintzis, V.A., Modeling of Flow and BOD Fate in Horizontal Subsurface Flow Constructed Wetlands, Chemical Engineering J. 200-202, 681-693 (2012)

[11] Waterloo Hydrogeologic Inc.: Visual MODFLOW v. 4.2. Users Manual, U.S. Geological Survey, Virginia, U.S.A (2006)

[12] Liolios, K., Tsihrintzis, V., Moutsopoulos, K., Georgiev, I., Georgiev. K., A Computational Approach for Remediation Procedures in Horizontal Subsurface Flow Constructed Wetlands, Lecture Notes in Computer Science 7116, 299-306 (2012)

[13] Liolios, K.A., Moutsopoulos, K.N., Tsihrintzis, V.A., Numerical Simulation of Phosphorus Removal in Horizontal Subsurface Flow Constructed Wetlands, Desalination and Water Treatment 56(5), 1282-1290 (2015)

[14] Zheng C. and Bennett G.D., Applied Contaminant Transport Modelling, 2nd Edition, Wiley, New York (2002).

Newton methods for option pricing with liquidity switching

Walter Mudzimbabwe, Carlos Vázquez

One of the assumptions made in the the classical Black-Scholes model for option pricing is that the market is liquid at all times. However, this is not the case in all markets, in which sometimes periods of liquidity are followed by time intervals where the market becomes illiquid. Recently, in Ludkovski and Shen [2], a model to price European options in a market that switches between liquid and illiquid states is proposed.

In the case of **European options**, p and q denote the indifference option prices in liquid and illiquid states, respectively. These difference option prices satisfy the following parabolic partial and ordinary differential equations system (see Ludkovski and Shen [2]), for details:

$$\frac{\partial p_i}{\partial t} + \frac{1}{2}\sigma_i^2 S^2 \frac{\partial^2 p_i}{\partial S^2} + \frac{\nu_{i1\text{-}i}}{\gamma}\frac{F_{1\text{-}i}}{F_i}(1 - e^{-\gamma(p_{1\text{-}i} - p_i)}) = 0, \tag{1}$$

where $i \in \{0,1\}, \sigma_0 = \sigma, \sigma_1 = 0$ and $p_0 = p, p_1 = q, p_i(T,S) = h(S)$, t and S represent time and underlying asset price, $\sigma > 0$ denotes the constant asset volatility and $\gamma > 0$ denotes the coefficient of risk aversion. Moreover, $F_0(t)$ and $F_1(t)$ are functions related to the investment performance and given in [2].

A weighted finite differences θ-method can now be written as

$$\begin{aligned}
&\frac{P_i^{j,n+1} - P_i^{j,n}}{\Delta t} + (1-\theta)\frac{1}{2}\sigma_i^2 S_j^2 D_+ D_- P_i^{j,n+1} + \theta\frac{1}{2}\sigma_i^2 S_j^2 D_+ D_- P_i^{j,n} \\
&+ (1-\theta)\frac{\nu_{i1-i}}{\gamma}\frac{F_{1-i}^{n+1}}{F_i^{n+1}}(1 - e^{-\gamma(P_{1-i}^{j,n+1} - P_i^{j,n+1})}) \\
&+ \theta\frac{\nu_{i1-i}}{\gamma}\frac{F_{1-i}^{n}}{F_i^{n}}(1 - e^{-\gamma(P_{1-i}^{j,n} - P_i^{j,n})}) = 0
\end{aligned} \tag{2}$$

for $j = 2, \cdots, M-1$ and $n = N-1, N-2, \cdots, 1$. At each time step t^n let:

$$\mathbf{x}^n = (P_0^{2,n}, \cdots, P_0^{M-1,n}, P_1^{2,n}, \cdots, P_1^{M-1,n}),$$

and the following notation

$$\nu_{i1-i}^n = \frac{\Delta t \nu_{i1-i}}{\gamma}\frac{F_{1-i}^n}{F_i^n}, \quad g_i^j(\mathbf{x^n}) = \exp(-\gamma(P_{1-i}^{j,n} - P_i^{j,n}))$$

and

$$\begin{aligned}
f_i^{j,n}(\mathbf{x}^n) = &-\theta L_i^j P_i^{j-1,n} + (1 + \theta D_i^j)P_i^{j,n} - \theta L_i^j P_i^{j+1,n} - \theta\nu_{i1-i}^n(1 - g_i^j(\mathbf{x^n})) \\
&- (1-\theta)L_i^j P_i^{j-1,n+1} - (1 - (1-\theta)D_i^j)P_i^{j,n+1} - (1-\theta)L_i^j P_i^{j+1,n+1} \\
&- (1-\theta)\nu_{i1-i}^{n+1}(1 - g_i^j(\mathbf{x^{n+1}})),
\end{aligned} \tag{3}$$

where

$$L_i^j = \alpha\sigma_i^2 S_j^2, \;\; D_i^j = 2\alpha\sigma_i^2 S_j^2, \;\; \alpha = \frac{1}{2}\frac{\Delta t}{(\Delta S)^2}.$$

Next we can introduce for each step n, the following nonlinear function:

$$\mathbf{f}^n(\mathbf{x}) = \left(f_0^{2,n}(\mathbf{x}), \cdots, f_0^{M-1,n}(\mathbf{x}), f_1^{2,n}(\mathbf{x}), \cdots, f_1^{M-1,n}(\mathbf{x})\right),$$

The problem is now to solve nonlinear system of equations:

$$\mathbf{f}^n(\mathbf{x}) = \mathbf{0}. \tag{4}$$

Thus, starting from $\mathbf{x}^{n,0} = \mathbf{x}^{n+1}$, at each iteration of Newton method we have to solve the linear system:

$$\mathbf{J}^n(\mathbf{x}^{n,k})\mathbf{\Delta}^{n,k} = -\mathbf{f}^n(\mathbf{x}^{n,k}), \;\; \mathbf{x}^{n,k+1} = \mathbf{x}^{n,k} + \mathbf{\Delta}^{n,k} \tag{5}$$

until convergence, where $\mathbf{J}^n(\mathbf{x}) \in \mathbf{R}^{2(M-2),2(M-2)}$ denotes the Jacobian of $\mathbf{f}^n$ at point $\mathbf{x}$,

$$\mathbf{J}^n = \begin{pmatrix} \mathbf{J}_0^n & \mathbf{D}_0^n \\ \mathbf{D}_1^n & \mathbf{J}_1^n \end{pmatrix},$$

where $\mathbf{J}_i^n(\mathbf{x}) \in \mathbf{R}^{M-2,M-2}$ is a tridiagonal matrix, the coefficients of which are given for $j, l = 1, \ldots, M-2$ by

$$\left(\mathbf{J}_i^n(\mathbf{x})\right)_{jl} = \begin{cases} 1 + \theta D_i^{j+1} + \theta\gamma\nu_{i1-i}^n g_i^{j+1}(\mathbf{x}) & \text{if} \quad j = l \\ -\theta L_i^{j+1} & \text{if} \quad j = l-1 \\ -\theta L_i^{j+1} & \text{if} \quad j = l+1 \\ 0 & \text{otherwise}, \end{cases}$$

and $\mathbf{D}_i^n(\mathbf{x}) \in \mathbf{R}^{M-2,M-2}$ is a diagonal matrix whose diagonal coefficients are given by

$$\left(\mathbf{D}_i^n(\mathbf{x})\right)_{jj} = -\theta\gamma\nu_{i1-i}^n g_i^{j+1}(\mathbf{x}), \quad j = 1, \ldots M-2.$$

Table 1: Indifference price p per option for buyer

	European call			Digital call		
Number of options	S_0=8	S_0=10	S_0=12	S_0=8	S_0=10	S_0=12
10	0.2879	1.0726	2.4482	0.1638	0.4199	0.6676
5	0.3133	1.1271	2.4877	0.1738	0.4348	0.6805
1	0.3227	1.1448	2.5020	0.1781	0.4412	0.6862

The order of convergence in variable S is computed as $O = \log_2\left(\frac{|u_M - u_{2M}|}{|u_{2M} - u_{4M}|}\right)$,. Although the problem is nonlinear, in all these experiments we observe a quadratic convergence in space.

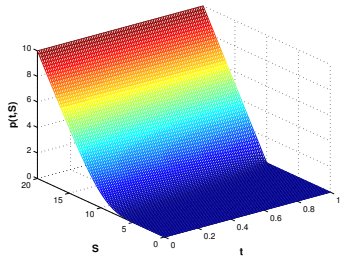

(a) p solution curve

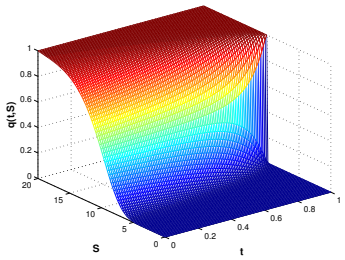

(b) q solution curve

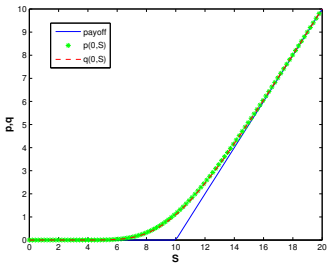

(c) Vanilla call p, q

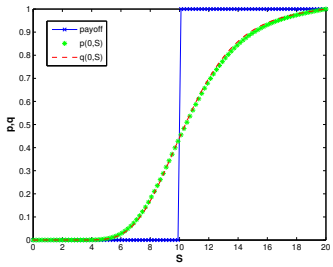

(d) Digital call p, q

Table 2: Order of convergence in S for p using implicit scheme, Digital call option

M	Value	Difference	Ratio	O
128	0.441346278059106	5.0969E-006	4.484722689	2.165018779
256	0.441351374942845	1.1365E-006	4.158038692	2.055903183
512	0.441352511442043	2.7333E-007	4.046247441	2.016584548
1024	0.441352784767830	6.7550E-008	4.013960169	2.005026301
2048	0.441352852318268	1.6829E-008	4.004761335	2.001716267
4096	0.441352869147144	4.2022E-009		
8192	0.441352873349361			

Table 3: Order of convergence in t for p using Crank-Nicholson scheme, Call option

N	Value	Difference	Ratio	O
128	1.145166992332569	6.1187E-007	4.032230375	2.011578067
256	1.145166380458687	1.5175E-007	4.017177866	2.006182340
512	1.145166228712922	3.7774E-008	4.008847272	2.003187455
1024	1.145166190938701	9.4227E-009	4.004558195	2.001643085
2048	1.145166181515987	2.3530E-009	4.001329503	2.000479437
4096	1.145166179162990	5.8805E-010		
8192	1.145166178574936			

American options give the holder the opportunity to exercise prior to the expiry. In mathematical terms, the problem becomes a free boundary problem. The problem can be written as the following discrete nonlinear complementary problem (NCP) (cf. [4])

$$\begin{cases} \mathbf{f}^n(\mathbf{x}^n) \geq \mathbf{0}, \\ \mathbf{x}^n \geq \mathbf{h} \\ (\mathbf{x}^n - \mathbf{h})^T \mathbf{f}^n(\mathbf{x}^n) = \mathbf{0}. \end{cases} \tag{6}$$

One of the most common way to price American options is to use the Projected Successive Over-Relaxation (PSOR) algorithm (see [6], for example). By applying PSOR technique at each Newton iterate to solve the corresponding linear complementarity problem (LCP) we get Newton-PSOR algorithm.
We also calculate the price of American options.

Table 4: Indifference price p per option for buyer

	American call			Digital call		
Number of options	S_0=8	S_0=10	S_0=12	S_0=8	S_0=10	S_0=12
10	0.2879	1.0726	2.4482	0.3478	0.9880	1.0000
5	0.3133	1.1270	2.4877	0.3757	0.9888	1.0000
1	0.3227	1.1448	2.5020	0.3828	0.9890	1.0000

Acknowledgement

This research was supported by the European Union under Grant Agreement number 304 617 (FP7 Marie Curie Action Project Multi-ITN Strike-Novel Methods in Computational Finance) and Bulgarian National Fund of Science under Project DFNI I02/20-2014.

References

[1] Leung T. S. T., *A Markov-modulated stochastic control problem with optimal multiple stopping with application to finance*, Decision and Control (CDC), IEEE, (2010), 559–566.

[2] Ludkovski M. and Shen Q., *European Option Pricing with Liquidity Shocks*, International Journal of Theoretic and Applied Finance **16** (2013), 219–249.

[3] Ortega, J. M. and Rheinboldt W. C., *Iterative solution of nonlinear systems of equations in several variables*, SIAM (2000).

[4] Pang J. S., *Newton's method for B-differential Equations*, Mathematics of Operations Research **15**(2) (1990), 311–341.

[5] Mudzimbabwe, W. and Vulkov, L., *IMEX schemes for a parabolic-ODE system of European options with liquidity shock*, J. Computational and Applied Mathematics, 299 (2016) 245-256.

[6] Wilmott P., Howison S. and Dewynne J., *The Mathematics of Financial Derivatives: A Student Introduction*, Cambridge University Press (1995).

Comparative analysis of finite elements for shear locking problems of Mindlin's plate

Stanislav Stoykov, Svetozar Margenov

1 Introduction

Plates are thin structures which have wide applications among engineering constructions. There are several hypothesis used to derive the two dimensional equation of equilibrium. The most common ones are Kirchhoff's and Mindlin's plate theories. Kirchhoff's hypothesis assumes that the transverse shear strains are negligible and it is applicable to thin plates. Mindlin's plate theory considers the transverse shear strains and it provides good results for thin and thick plates. Both theories assume linear variation of the in-plane displacements with the thickness coordinate. There are also higher order plate theories which express the variation of the in-plane displacements by higher order functions.

Mindlin's plate theory is the most commonly used, the resulting PDE is of second order and the related finite element discretization requires C^0 continuity. This approach leads to shear locking when the plate is thin. There are several techniques to avoid shear locking, such as reduced and selective integration, mixed formulation or approximation by higher order shape functions. The aim of the current paper is to implement the most commonly used finite elements and to investigate their behavior when they are applied to thin plates.

2 MindlinâĂŹs plate equation of motion

A rectangular plate of isotropic material and uniform thickness d is considered for the computational analysis. The dimensions of the plate along x and y axes are denoted by a and b respectively. The transverse displacement on the middle plane is denoted by $w(x, y)$ and $\phi_x(x, y)$ and $\phi_y(x, y)$ represent the rotations of the middle plane about x and y axes. The equilibrium equations have the following form [1]:

$$\begin{aligned} \lambda A_{55}\left(\frac{\partial^2 w}{\partial x^2}+\frac{\partial \phi_y}{\partial x}\right)+\lambda A_{44}\left(\frac{\partial^2 w}{\partial y^2}+\frac{\partial \phi_x}{\partial y}\right) &= -q(x,y) \\ D_{66}\frac{\partial^2 \phi_x}{\partial x^2}+(D_{12}+D_{66})\frac{\partial^2 \phi_y}{\partial x \partial y}+D_{22}\frac{\partial^2 \phi_x}{\partial y^2}-\lambda A_{44}\left(\frac{\partial w}{\partial y}+\phi_x\right) &= 0 \\ D_{11}\frac{\partial^2 \phi_y}{\partial x^2}+(D_{12}+D_{66})\frac{\partial^2 \phi_x}{\partial x \partial y}+D_{66}\frac{\partial^2 \phi_y}{\partial x^2}-\lambda A_{55}\left(\frac{\partial w}{\partial x}+\phi_y\right) &= 0 \end{aligned} \tag{1}$$

Here D_{ij} are the stiffness coefficients, i.e. they relate the moment resultants with the curvatures and define the bending stiffness matrix, A_{44} and A_{55} formulate the transverse shear stiffness matrix and λ is the shear correction factor. Simply-supported

boundary conditions on all four edges are considered:

$$\begin{aligned} w = 0, \frac{\partial \phi_y}{\partial x} = 0, \phi_x = 0, \quad \text{for} \quad x = 0, a, \\ w = 0, \frac{\partial \phi_x}{\partial y} = 0, \phi_y = 0, \quad \text{for} \quad y = 0, b. \end{aligned} \tag{2}$$

The strain energy is defined by the following expression:

$$U = \frac{1}{2} \int_V (\sigma_x \epsilon_x + \sigma_y \epsilon_y + \tau_{xy}\gamma_{xy} + \tau_{yz}\gamma_{yz} + \tau_{xz}\gamma_{xz}) dV \tag{3}$$

which, under the assumptions of MindlinâĂŹs plate theory, and after integration with respect to the transverse axis z, has the following form:

$$\begin{aligned} U = \frac{1}{2} \frac{Ed^3}{12(1-\nu^2)} \int_\Omega \left(\left(\frac{\partial \phi_y}{\partial x} \right)^2 + 2\nu \frac{\partial \phi_y}{\partial x} \frac{\partial \phi_x}{\partial y} + \left(\frac{\partial \phi_x}{\partial y} \right)^2 + \right. \\ \left. \frac{1-\nu}{2} \left(\frac{\partial \phi_y}{\partial x} + \frac{\partial \phi_x}{\partial y} \right)^2 + \frac{6\lambda(1-\nu)}{d^2} \left(\left(\frac{\partial w}{\partial y} + \phi_x \right)^2 + \left(\frac{\partial w}{\partial x} + \phi_y \right)^2 \right) \right) \end{aligned} \tag{4}$$

E is the Young modulus of the material and ν is the Poisson's ratio. For plates with small thickness, the coefficient $\frac{6\lambda(1-\nu)}{d^2}$ becomes much larger than the other coefficients from the strain energy. Since the minimum of U is sought, this forces $\frac{\partial w}{\partial y} \to -\phi_x$ and $\frac{\partial w}{\partial x} \to -\phi_y$ as $d \to 0$, i.e.

$$\begin{aligned} \lim_{d \to 0} \int_\Omega \left(\frac{\partial w}{\partial y} + \phi_x \right)^2 d\Omega \to 0, \\ \lim_{d \to 0} \int_\Omega \left(\frac{\partial w}{\partial x} + \phi_y \right)^2 d\Omega \to 0. \end{aligned} \tag{5}$$

These enforcements introduce additional constraints in the finite element model which leads to reduced order of convergence. This phenomenon is known as shear locking. As a result of the shear locking, the plate becomes stiff and the displacements become smaller compared to the true solution. The terms in eq. (5) are related with the shear strain energy and they employ zero shear stress on the limit of very thin plates.

3 Comparison of different finite elements

Several finite elements are compared in order to investigate their behavior as the thickness of the plate becomes small. The considered elements are presented in Fig.1 using digital codes for simplicity of the notations. Element **404** has four nodes on the corners, it uses four bilinear shape functions and it uses selective and reduced integration for the shear strain energy. This element is equivalent to the mixed FEM with piecewise constant approximation of the shear forces. Element **408** has eight nodes, placed on the corners and on middle of the edges. The element uses quadratic

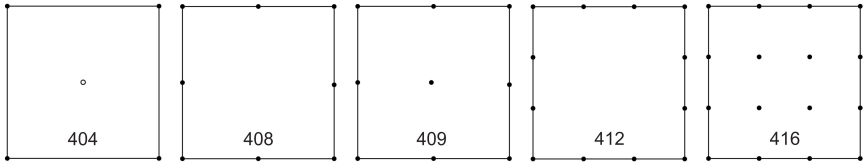

Figure 1: Types of finite elements used in the comparative analysis.

shape functions. This element belongs to the Serendipity family of elements. Element **409** has nine nodes, it uses biquadratic shape functions. The element belongs to the Lagrange family of elements. Element **412** is the cubic element from Serendipity family. Element **416** is the cubic element from Lagrange family.

Plate with dimensions $a = 0.6$ m and $b = 0.3$ m and material properties: $E = 70$ GPa and $\nu = 0.3$ is assumed for the numerical experiments. Uniformly distributed load of 40 N/m^2 is applied in transverse direction. Shear correction factor $\lambda = 5/6$ is used. Different meshes are considered, each one is obtained from the previous one by dividing the edges of the elements by 2. The first three meshes are shown in Fig. 2. The energy norm due to static load is computed for the different meshes and for different thicknesses of the plate. The relative error of the solution in energy norm obtained by the different finite elements is presented in Fig. 3 as a function of the plate thickness. The results confirm that elements 409 and 416 are robust and behave well when the thickness of the plate is small. The rate of convergence of these elements is reduced due to the locking effect. Elements 408 and 412 are not robust, the results show that they can produce enormous error, thus they are not reliable for plate problems. Element 404 used with selective and reduced integration is robust, it gives convergence of order $O(h)$ in energy norm.

The error in energy norm of mesh i is denoted by $\|e_i\| = \left\|u - u_i^h\right\|$. The ratio of the errors in energy norms of two sequential meshes of element 409 are presented in Table 1. Considering the theoretical estimation presented in [2], element 409 has locking order of $1/2$ in energy norm which is confirmed by the results in Table 1. For thick plates, the convergence order for sufficiently fine meshes is close to the theoretical estimation of second order PDE without any locking - $O(h^2)$, while when the thickness is reduced, the convergence becomes of order $O(h)$.

Table 1: Ratio of errors in energy norms of element 409.

409	$\frac{\|e_{m1}\|}{\|e_{m2}\|}$	$\frac{\|e_{m2}\|}{\|e_{m3}\|}$	$\frac{\|e_{m3}\|}{\|e_{m4}\|}$	$\frac{\|e_{m4}\|}{\|e_{m5}\|}$	$\frac{\|e_{m5}\|}{\|e_{m6}\|}$
$d = 0.005$	2.0369	2.3748	2.9723	3.5813	3.9955
$d = 0.001$	1.9270	2.0005	2.0750	2.2865	2.8793
$d = 0.0001$	1.9225	1.9824	2.0045	2.0391	2.1875

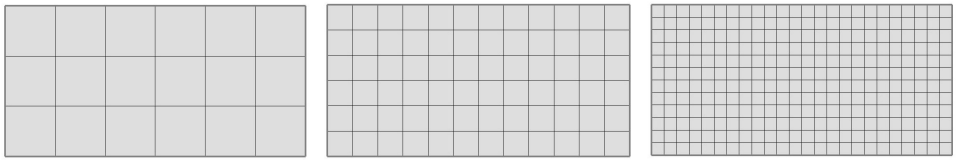
Figure 2: Meshes of rectangular finite elements with different sizes, Mesh 1 Δh = 0.1, Mesh 2 Δh = 0.05, Mesh 3 Δh = 0.025.

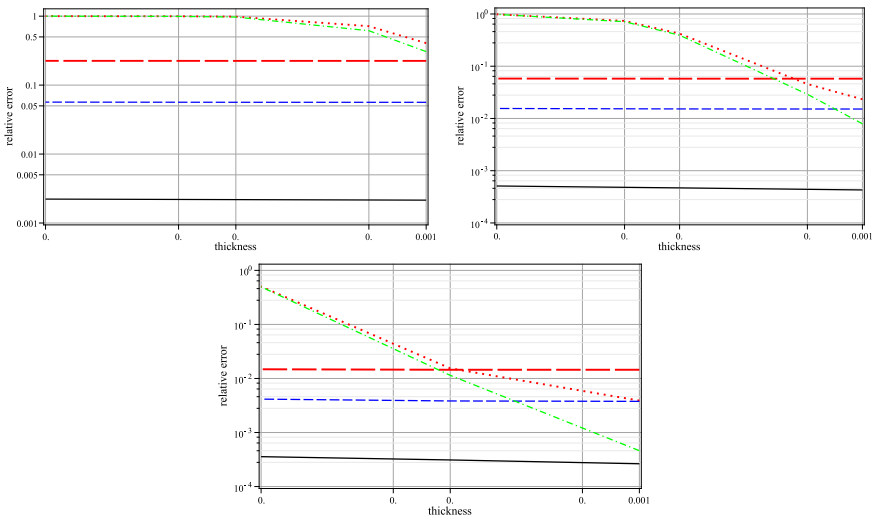

Figure 3: Logarithmic plots of relative error of the energy norm of the different finite elements, (a) Mesh 1, (b) Mesh 2, (c) Mesh 3. — — — 404, · · · · · 408, - - - 409, — · — · — 412, —— 416

4 Conclusion

Five different rectangular finite elements are developed and applied to the numerical solution of the Mindlin's plate equation of equilibrium. The behavior the finite elements is investigated for different meshes and thicknesses of the plate. It is shown that the elements from the Lagrange family are robust while the ones from Serendipity family are not and produce enormous error when the thickness is decreasing. The bilinear element with selective and reduced integration is free of locking and provides good results and has less degrees of freedom.

Acknowledgments

This work was supported by the Bulgarian Academy of Sciences through the "Young Scientists" Grant No. DFNP-93/04.05.2016.

References

[1] H. Altenbach, J. Altenbach, and W. Kissing. *Structural Analysis of Laminate and Sandwich Beams and Plates*. Lublin, 2001.

[2] M. Suri, I. Babuska, and C. Schwab. Locking effects in the finite element approximation of plate models. *Mathematics of computation*, 64:461–482, 1995.

Interpolation of Convex Scattered Data in $\mathbb{R}^3$ using Piecewise Quadratic Minimum Norm Networks

Krassimira Vlachkova

Scattered data interpolation is a fundamental problem in approximation theory and finds applications in many areas including geology, medicine, architecture, computer graphics, etc. Different methods for solving this problem were applied and reported, excellent surveys can be found e.g., in [4, 5]. The problem can be formulated as follows: Given *scattered data* $(x_i, y_i, z_i) \in \mathbb{R}^3$, $i = 1, \ldots, N$, that is points $\mathbf{v}_i = (x_i, y_i)$ are different and non-collinear, find a bivariate function F defined in a certain domain D containing points $\mathbf{v}_i$, such that F possesses continuous partial derivatives up to a given order and $F(x_i, y_i) = z_i$.

One of the possible approaches to solving the problem is due to Nielson [6]. The method consists of the following three steps:

Step 1. Triangulation. Construct a triangulation T of $\mathbf{v}_i,\ i = 1, \ldots N$.

Step 2. Minimum norm network (MNN). The interpolant F and its first order partial derivatives are defined on the edges of T so as to satisfy an extremal property. The MNN is a cubic curve network, i. e. on every edge of T it is a cubic polynomial.

Step 3. Interpolation surface. The obtained network is extended to F by an appropriate *blending method*. The interpolant is a rational function on every triangle in T.

In [1] Andersson et al. gave an alternative proof of Nielson's result. Their method allows to consider and handle the case where the data are convex and a convex interpolant is sought. Andersson et al. formulated and solved the corresponding extremal constrained interpolation problem of finding a MNN that is convex along the edges of the triangulation. The results from [1] are extended in [7] to the class of L_p-norms for $1 < p \leq \infty$. The extremal constrained interpolation problem for $p = \infty$ has a solution whose restriction to any edge e in T is a convex quadratic spline function with at most one knot in the interval $(0, \|e\|)$, see Fig. 1. We note that the edge convex MNN may not be globally convex. Moreover, even in the case where it is globally convex, Nielson's blending method may produce non-convex surface.

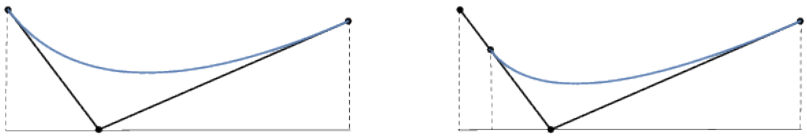

a. **b.**

Figure 1: The edge convex MNN for $p = \infty$ on every edge of T is either a quadratic polynomial (**a.**) or a C^1-continuous spline with one inner knot consisting of a linear function plus a quadratic polynomial (**b.**)

We consider the interpolation of convex scattered data in $\mathbb{R}^3$ associated with a planar triangulation T. Convexity preserving methods using macro-element splines defined on triangulations has been developed e. g., in [2, 3]. We propose a solution that constructs a minimum norm piecewise quadratic network defined and convex on the edges of T and then builds a Powell-Sabin six-split interpolant. We obtain necessary and sufficient geometric conditions for the convexity of the resulting interpolant. An example of a triangulation T, the corresponding edge convex MNN for $p = \infty$, and the convex Powell-Sabin six-split interpolant are shown in Fig. 2. The data are $(-1/2, -\sqrt{3}/6, 0)$, $(1/2, -\sqrt{3}/6, 0)$, $(0, \sqrt{3}/3, 0)$, $(0, 0, -1/2)$.

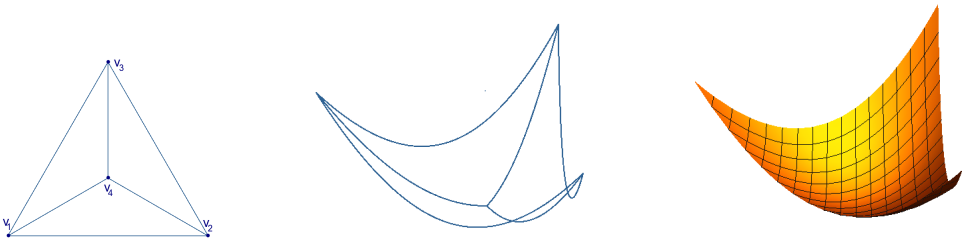

Figure 2: Triangulation T, the edge convex MNN for $p = \infty$, and the corresponding convex Powell-Sabin six-split interpolant.

Acknowledgments. This work is partially supported by Sofia University Science Fund Grant No. 48/2016.

References

[1] Andersson, L.-E, Elfving, T., Iliev, G., Vlachkova, K., 1995. Interpolation of convex scattered data in $\mathbb{R}^3$ based upon an edge convex minimum norm network. J. of Approx. Theory, 80(3), 299-320.

[2] Carnicer, J.M., Dahmen, W., 1992. Convexity preserving interpolation and Powell-Sabin elements. Comput. Aided Geom. Design, 9 (4), 279-289.

[3] Carnicer, J.M., Goodman, T.N.T., Peña, J.M., 2009. Convexity preserving scattered data interpolation using Powell-Sabin elements. Comput. Aided Geom. Design, 26 (2), 779-796.

[4] Franke, R., Nielson, G.M, 1991. Scattered data interpolation and applications: A tutorial and survey In: Hagen, H., Roller, D. (Eds.). Geometric Modeling. Springer, Berlin Heidelberg, pp. 131-160.

[5] Lodha, S.K., Franke, R., 1997. Scattered data techniques for surfaces, in: Hagen, H, Nielson, G.M., Post, F. (Eds.). In: Proceedings of Dagstuhl Conference on Scientific Visualization. IEEE Computer Society Press. Washington, DC, pp. 182-222.

[6] Nielson, G.M., 1983. A method for interpolating scattered data based upon a minimum norm network. Math. Comp., 40 (161), 253-271.

[7] Vlachkova, K., 1992. Interpolation of convex scattered data in $\mathbb{R}^3$ based upon a convex minimum L_p-norm network. C. R. Acad. Bulg. Sci. 45 (12), 13-15.

Part B

List of participants

Emanouil Atanassov
Institute of Information and
Communication Technologies
Bulgarian Academy of Sciences
Acad. G. Bontchev Str., bl. 25A
1113 Sofia, Bulgaria
emanouil@parallel.bas.bg

Owe Axelsson
Institute of Geonics AS CR
Studentska 1768
70800 Ostrava, Czech Republic
owea@it.uu.se

Todor Balabanov
Institute of Information and
Communication Technologies
Bulgarian Academy of Sciences
Acad. G. Bontchev Str., Bl. 2
1113 Sofia, Bulgaria
todorb@iinf.bas.bg

Gergana Bencheva
Institute of Information and
Communication Technologies
Bulgarian Academy of Sciences
Acad. G. Bontchev Str., bl. 25A
1113 Sofia, Bulgaria
gery@parallel.bas.bg

Gabriel Dimitriu
"Gr. T. Popa" University of
Medicine and Pharmacy
Universitatii Str. 16
700115 Iasi, Romania
dimitriu.gabriel@gmail.com

Stefka Dimova
Faculty of Mathematics and Informatics
Sofia University
5 James Bourchier Blvd.
1164 Sofia, Bulgaria
dimova@fmi.uni-sofia.bg

Stefka Fidanova
Institute of Information and
Communication Technologies
Bulgarian Academy of Sciences
Acad. G. Bonchev Str., bl. 25A
1113 Sofia, Bulgaria
stefka@parallel.bas.bg

Mihail Galabov
Institute of Information and
Communication Technologies
Bulgarian Academy of Sciences
Acad. G. Bonchev Str., bl. 25A
1113 Sofia, Bulgaria
mishogal@gmail.com

Krassimir Georgiev
Institute of Information and
Communication Technologies
Bulgarian Academy of Sciences
Acad. G. Bonchev Str., bl. 25A
1113 Sofia, Bulgaria
georgiev@parallel.bas.bg

Ivan Georgiev
Institute of Information and
Communication Technologies &
Institute of Mathematics and Informatics
Bulgarian Academy of Sciences
Acad. G. Bonchev Str., bl. 25A
1113 Sofia, Bulgaria
ivan.georgiev@parallel.bas.bg

Irina Georgieva
Institute of Mathematics and Informatics
Bulgarian Academy of Sciences
Acad. G. Bonchev Str., bl. 8
1113 Sofia, Bulgaria
irina@math.bas.bg

Silvia Grozdanova
Institute of Information and
Communication Technologies
Bulgarian Academy of Sciences
Acad. G. Bonchev Str., bl. 25A
1113 Sofia, Bulgaria
silvia@parallel.bas.bg

Stanislav Harizanov
Institute of Information and
Communication Technologies
Bulgarian Academy of Sciences

Acad. G. Bonchev Str., bl. 25A
1113 Sofia, Bulgaria
sharizanov@parallel.bas.bg

Clemens Hofreither
Johannes Kepler University Linz
Altenbergerstr. 69
4040 Linz, Austria
chofreither@numa.uni-linz.ac.at

Nevena Ilieva
Institute of Information and
Communication Technologies
Bulgarian Academy of Sciences
Acad. G. Bonchev Str., bl. 25A
1113 Sofia, Bulgaria
nevena.ilieva@parallel.bas.bg

Miglena Koleva
Ruse University
Studentska Str. 8
7017 Ruse, Bulgaria
mkoleva@uni-ruse.bg

Nikola Kosturski
Institute of Information and
Communication Technologies
Bulgarian Academy of Sciences
Acad. G. Bonchev Str., bl. 25A
1113 Sofia, Bulgaria
kosturski@parallel.bas.bg

Raytcho Lazarov
Texas A&M University
Deaprtment of Mathematics
77843 College Station, Texas, USA
lazarov@math.tamu.edu

Elena Lilkova
Institute of Information and
Communication Technologies
Bulgarian Academy of Sciences
Acad. G. Bonchev Str., bl. 25A
elilkova@parallel.bas.bg

Angelos Liolios
Democritus University of Thrace
Dept. of Civil Engineering
L. Pirgou 35 B
67100 Xanthi, Greece
aliolios@civil.duth.gr

Konstantinos Liolios
Institute of Information and
Communication Technologies
Bulgarian Academy of Sciences
Acad. G. Bontchev str., bl. 25A
1113 Sofia, Bulgaria
kostisliolios@gmail.com

Ivan Lirkov
Institute of Information and
Communication Technologies
Bulgarian Academy of Sciences
Acad. G. Bonchev Str., bl. 25A
1113 Sofia, Bulgaria
ivan@parallel.bas.bg

Svetozar Margenov
Institute of Information and
Communication Technologies
Bulgarian Academy of Sciences
Acad. G. Bonchev Str., bl. 25A
1113 Sofia, Bulgaria
margenov@parallel.bas.bg

Walter Mudzimbabwe
Ruse University
Studentska Str. 8
7017 Ruse , Bulgaria
wmudzimbabwe@uni-ruse.bg

Stanislav Stoykov
Institute of Information and
Communication Technologies
Bulgarian Academy of Sciences
Acad. G. Bonchev Str., bl. 25A
1113 Sofia, Bulgaria
stoykov@parallel.bas.bg

Venelin Todorov
Institute of Information and
Communication Technologies
Bulgarian Academy of Sciences
Acad. G. Bonchev Str., bl. 25A
1113 Sofia, Bulgaria

venelinltodorov@gmail.com

Krassimira Vlachkova
Faculty of Mathematics and Informatics
Sofia University
5 James Bourchier Blvd.
1164 Sofia, Bulgaria
krassivl@fmi.uni-sofia.bg

Lubin Vulkov
Ruse University
Studentska Str. 8
7017 Ruse , Bulgaria
lvalkov@uni-ruse.bg

Yavor Vutov
Institute of Information and
Communication Technologies
Bulgarian Academy of Sciences
Acad. G. Bonchev Str., bl. 25A
1113 Sofia, Bulgaria
yavor@parallel.bas.bg

Zahari Zlatev
Aarhus UniversityÂă
Frederiksborgvej 399, P. O. Box 358Âă
4000 Roskilde, Denmark
zz@envs.au.dk